Electronic Supplementary Material (ESI) for Catalysis Science & Technology.
This journal is © The Royal Society of Chemistry 2021

Electronic Supplementary Information: The Role of Site Coordination on the CO_2 Electro-reduction Pathway on Stepped and Defected Copper Surfaces

Lucas G. Verga ,* Paulo C. D. Mendes,* Vivianne K. Ocampo-Restrepo,* and Juarez L. F. Da Silva*

São Carlos Institute of Chemistry, University of São Paulo, PO Box 780, 13560-970, *São Carlos, SP, Brazil*

E-mail: lucas.gverga@gmail.com; paulaocdm@gmail.com; vivianne.o.restrepo@gmail.com; juarez_dasilva@iqsc.usp.br

Contents

S1 Introduction

As indicated in the contents, the electronic supplementary information is separated into several sections containing the following information:

1. Convergence calculations for Cu bulk, Section S2, and Cu surfaces, Section S3.
2. Additional details about the calculated Cu_3/Cu(533) surfaces, Section S4.
3. Results about all distinct structures obtained for the calculations of CO_2 reduction intermediates interacting with Cu surfaces, Section S5.
4. Results for the terms from vibrational calculations, Section S6.
5. Examples of the calculation of reaction energy diagrams, Section S7, and the reaction energy diagrams calculated for different applied potentials, Section S8

S2 Cu Bulk Convergence Tests

The lattice parameter for face-centered cubic (fcc) copper was obtained after convergence calculations for the plane-wave kinetic energy cutoff and **k**-point sampling. Here, as well as in the entire manuscript, all the calculations were performed using the projector augmented wave (PAW) method,[1,2] the PBE[3] functional, and Grimme D3 corrections.[4]

To test the convergence with respect to the plane-wave cutoff energy, we have used a $(20\times20\times20)$ **k**-mesh. For each value of kinetic energy cutoff, we have performed the volume relaxation several times using the output lattice parameter of the last minimization step as the input for the subsequent one. This procedure was performed until the initial and final lattice parameters were the same and the results can be observed in Figure S1. The same test was performed to analyze the lattice parameter convergence with respect to the **k**-mesh, maintaining the kinetic energy cutoff as 834 eV.

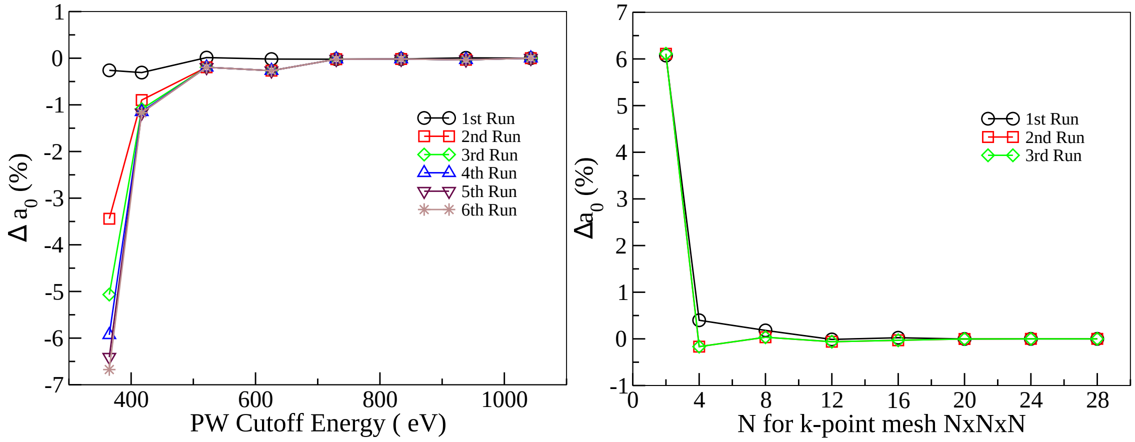

Figure S1: Lattice parameter variation in (%) versus the plane-wave kinetic energy cutoff and **k**-mesh for an fcc copper Bulk.

Using the converged lattice parameter of 3.56 Å, we have computed the density of states and the angular momentum projected density of states for the copper bulk. Figure S2 shows the total, local, and interstitial DOS, as well as the angular momentum projected DOS, with the *d*-band upper edge being almost 2 eV below the Fermi level, as expected for such *d*-filled metal.

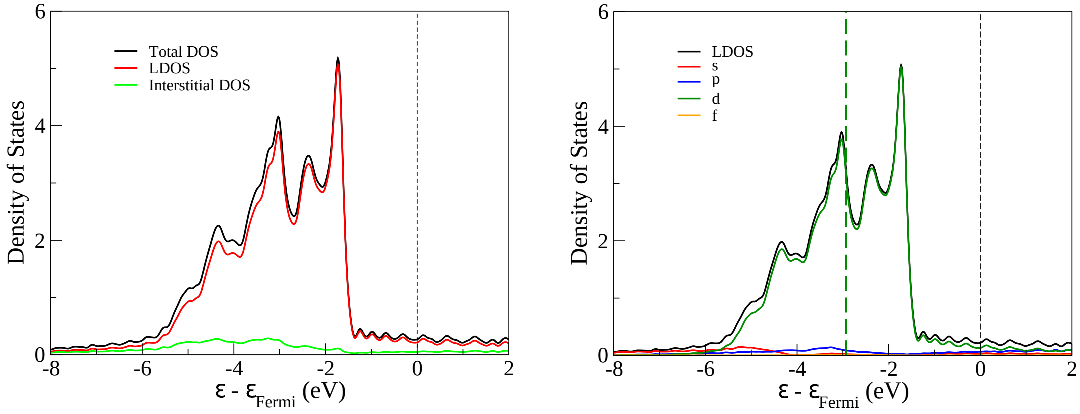

Figure S2: Total, local, and interstitial density of states obtained for an fcc bulk of copper, as well as the angular momentum projected density of states for the same system. The segmented black line indicates the Fermi level, while the green line shows the *d*-band center which is widely used as a descriptor for adsorption energies when obtained for metallic surfaces.

S3 Metallic Surfaces: Cu(111), Cu(100), Cu(110)

Using the optimized lattice parameter, we have constructed Cu(111), Cu(100) and Cu(110) surfaces. We have tested, how certain surface properties change as we change from one surface to another and also with respect to the kinetic energy cutoff, **k**-point mesh, vacuum thickness, and number of layers in the slab model. We have calculated surface energies, σ, work function, Φ, and variations in the inter-layer spacing for different surfaces, where the surface energies were defined as:

$$\sigma = \frac{1}{2}(E_{tot}^{Slab} - NE_{tot}^{Bulk}) \,, \tag{1}$$

where, E_{tot}^{Slab} and E_{tot}^{Bulk} are the total energies obtained from a slab and a Bulk calculation, and N is the number of layers in the slab model. Meanwhile, the work function of a surface was defined as the difference between the electrostatic potential in the vacuum (distant from the surface) and the Fermi level, as follows:

$$\Phi = V_{pot}(r_{vac}) - E_{Fermi} \,. \tag{2}$$

Finally, we have also computed the percentage of the variation in the inter-layer distances:

$$\Delta d_{i,j} = 100 \times (d_{i,j} - d_0/d_0) \,, \tag{3}$$

where, $d_{i,j}$ is the distance between the layers i and j, and d_0 is the inter-layer spacing obtained from a bulk calculation (frozen surface).

Firstly, we have performed plane-wave energy cutoff and **k**-mesh convergence tests for the inter-layer spacing, work functions, and surface energies of a (1×1) Cu(111) surface with 7 layers. For the kinetic energy cutoff convergence tests, we have employed a $(20 \times 20 \times 1)$ **k**-mesh, while for the **k**-mesh test, we have used a 469.17 eV kinetic energy cutoff. Figure S3 shows the results of the convergence tests, where we have observed that a 469.17 eV and a $(12 \times 12 \times 1)$ **k**-mesh is enough to get properties converged to an acceptable level.

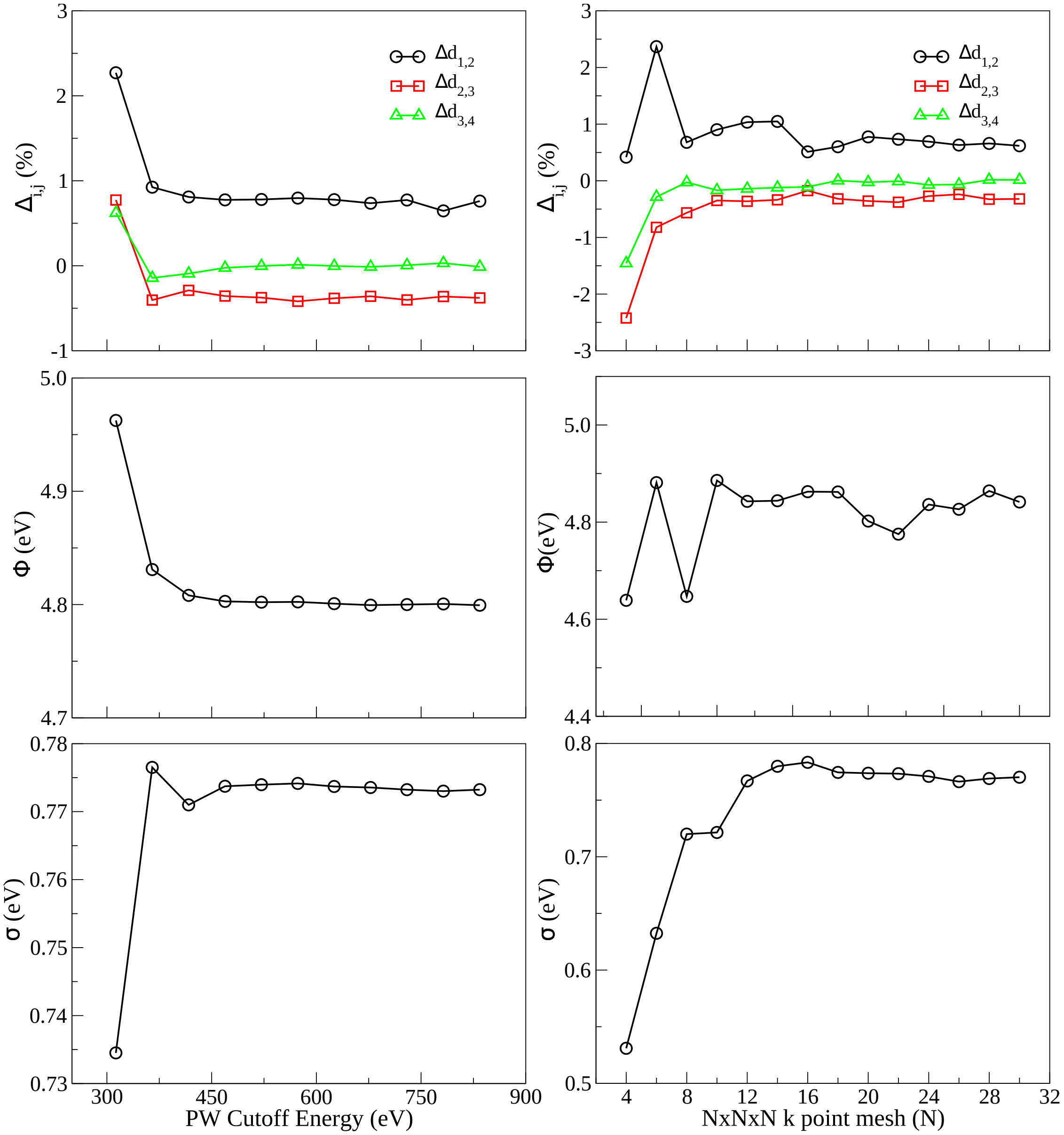

Figure S3: Change in inter-layer spacing, work functions, and surface energies for a (1 × 1) Cu(111) surface with 7 layers as a function of the plane-wave energy cutoff and the **k**-mesh.

We have also computed the surface energies, work functions and inter-layer spacing for Cu(111) slabs with different number of layers, varying from 2 to 15. We have observed that depending on the level of precision required for a given analysis, 5 to 8 layers is enough to get well-converged interlayer spacings and workfunction values.

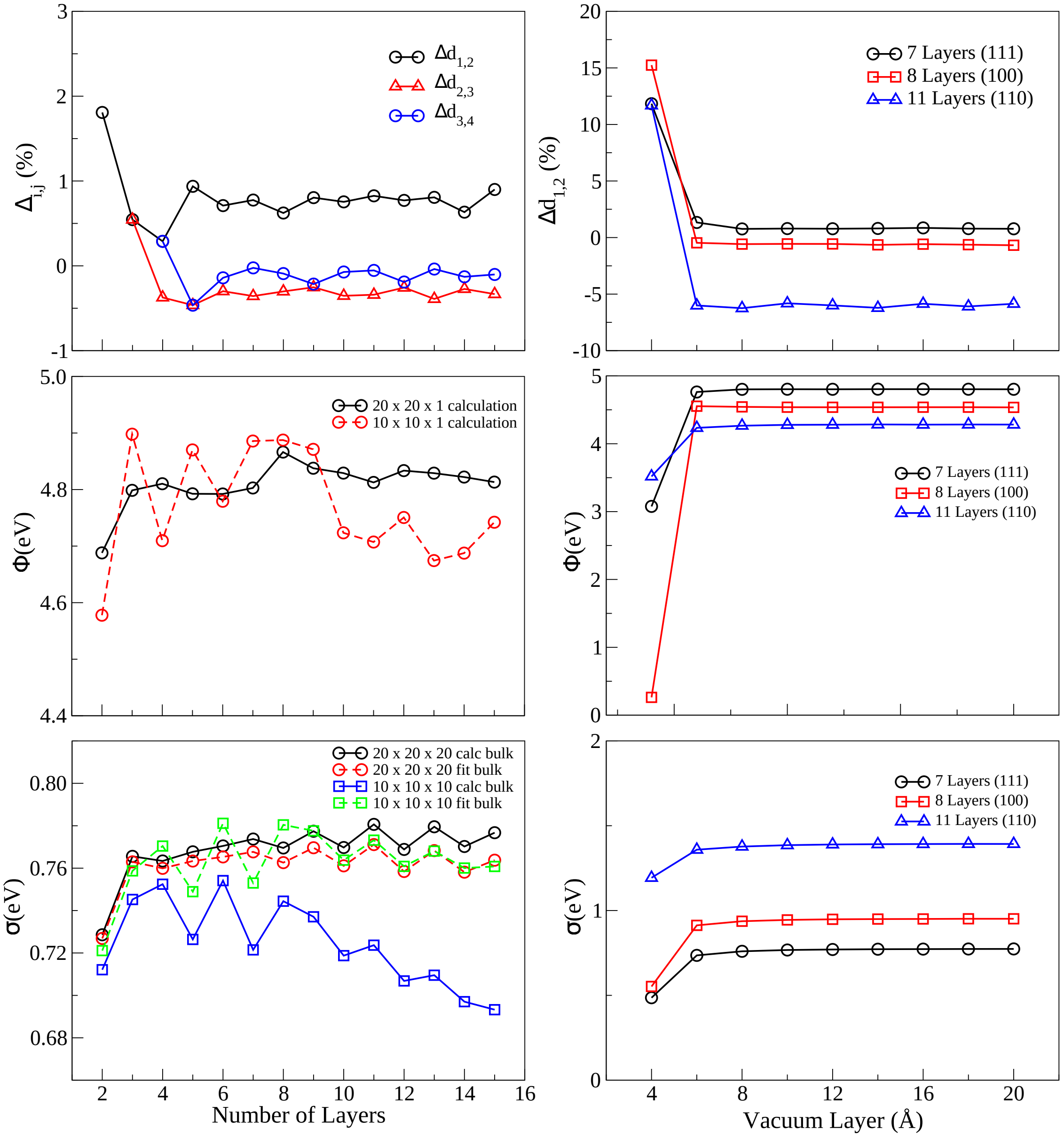

Figure S4: Change in inter-layer spacing, work functions, and surface energies for a Cu(111) as a function of the number of layers. Surface energies, inter-layer spacing and work functions for different copper surfaces. Change in surface energies and work function for a Cu(111) as a function of the size of the vacuum gap.

Meanwhile, surface energies as a function of the number of layers are more subtle to obtain. This quantity requires energies from two separate calculations (Slab and Bulk) and, as we can observe in equation 1, the error associated with the bulk calculation increases with the number of layers leading to a divergent behavior. As suggested in the literature,[5] we have tested computing E_{tot}^{Bulk} as the slope of E_{tot}^{Slab} vs the number of layers. As shown in Figure S4, when such strategy is employed, we avoid the divergent behavior and obtain surface energy convergence with the number of layers. We also show, that another solution is to obtain the energies for both cases with highly converged calculations, which also yields converged properties.

We have performed the same calculations for Cu(100) and Cu(110) surfaces with 8 and 11 layers, respectively. For these calculations, we have used a $(20\times 20\times 1)$ **k**-mesh for Cu(100) and $(20\times 14\times 1)$ for Cu(110) calculations. For all surfaces, we have tested how the vacuum layer added between periodic slabs along the z direction affects the calculated surface properties. The results in figure S4 shows that a vacuum layer of around 10 Å is sufficient to obtain well converged properties.

Table S1: Surface energies, inter-layer spacing and work functions for different copper surfaces.

	Cu(111)			Cu(100)			Cu(110)		
	PBE +D3	PBE	Exp.	PBE +D3	PBE	Exp.	PBE +D3	PBE	Exp.
Δd_{12} (%)	0.92	−0.6 [6]	−0.7 [7]	−0.57	−2.9 [6]	−1.1 [8]	−6.25	−9.7 [6]	-10 ± 2.5[8]
σ (eV)	0.77	0.50 [5]		0.95	0.60 [9]		1.39	0.90 [9]	
Φ (eV)	4.80	4.78 [5]	4.98 [10]	4.53	4.39 [11]	4.59 [10]	4.28	4.18 [11]	4.48 [10]

Finally, we have used the optimal set of parameters obtained through the convergence calculations to asses how the values calculated with our strategy using a PBE exchange correlation functional with Grimme D3 dispersion, was comparable to experiments and other theoretical work. As the surface energies are a measure of the energy needed to cut a bulk material into a slab along a certain crystal plane, the inclusion of the attractive dispersion interaction increases the calculated surface energy values for all surfaces. We have also observed that the largest relaxations happened for the more open Cu(110) surface, and that the surface energies are ordered as Cu(111) < Cu(100) < Cu(110), while work functions are Cu(111) > Cu(100) > Cu(110) which is similar to what we observe from the literature, with more closed surfaces being more stable and presenting larger work functions.

S4 Construction of Cu_3/Cu(533)

As discussed in the manuscript, we have constructed Cu_3/Cu(533) surfaces to explore the effect of low-coordinated sites for the CO_2 reduction on Cu surfaces. The definition of the Cu_3 cluster position on the Cu(533) surface was made after optimizing the trimer on different regions. We have considered a triangular, $Cu_3{}^T$, under the Cu(533) step and in the terrace near the surface step, with each Cu atom located on an FCC site. For the terrace regions, we have also tested top, bridge, and HCP adsorption sites. We have also included a linear $Cu_3{}^L$ trimer using FCC sites perpendicular to the surface steps, which will not be useful for our study on adsorption of CO_2 intermediates, but could be interesting for further studies about defected Cu surfaces. All the initial surfaces are summarized in the Figure S5, while discussions about the surface properties can be found in the main text.

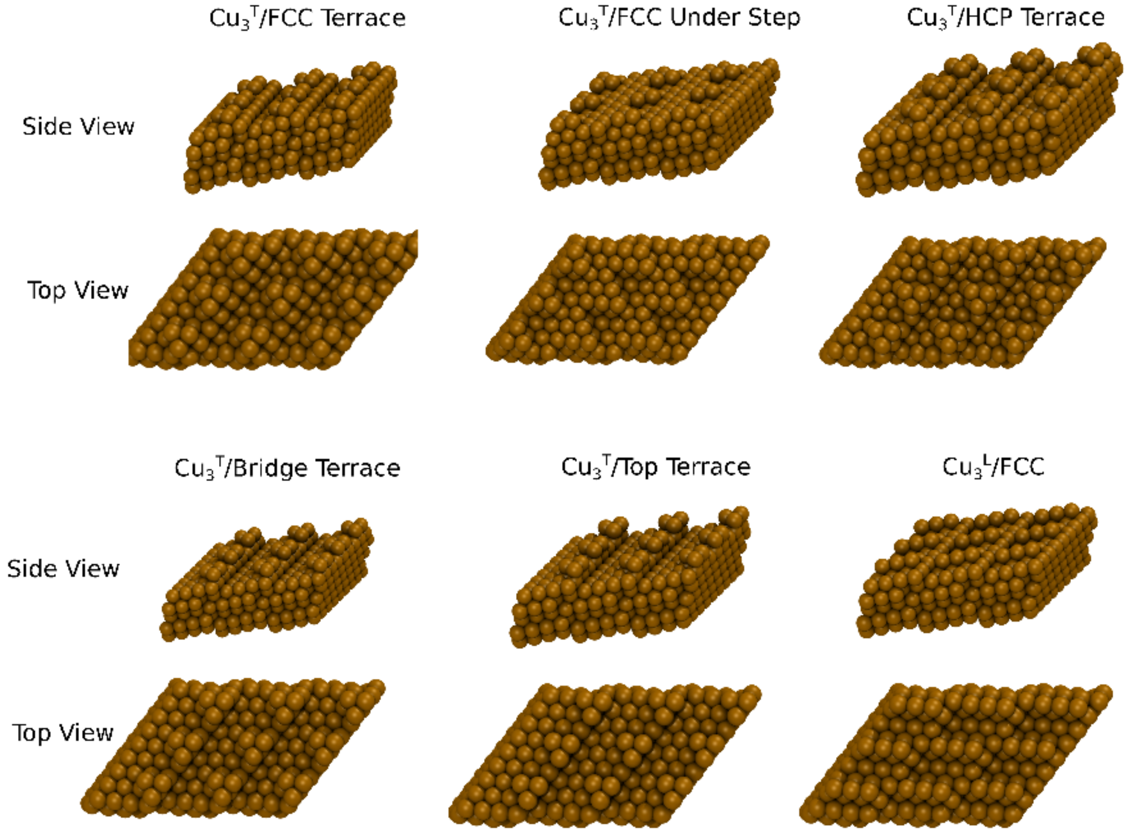

Figure S5: Initial Cu_3/Cu(533) structures considered in the present study.

S5 Adsorption of CO_2 Reduction Intermediates on Cu Sites of Different Coordination

We have placed the adsorbates on different adsorption sites (top, bridge, and hollow) and different orientations of the molecule with respect to the surfaces. Here, we show all the distinct configurations obtained for each adsorbate after geometry optimizations. Several characteristics of each adsorbate and adsorbate-surface interactions control the number of resulting structures present here, e.g., adsorbates such as COOH are stabilized with a larger number of orientations with respect to the surface, either with a C–O or a C–OH bond parallel to the surface, than an adsorbate such as CO, which always adsorbs via the C atom in Cu surfaces. Similarly, for certain adsorbates, such as C, calculations that started on top or bridge site are optimized to result in structures on hollow sites, which leads to a smaller number of distinct configurations.

In addition to the adsorption, E_{ad}, and interaction energies, E_{int}, we also present energetic quantities to address the deformations happening in the molecules, ΔE^{Mol}, and substrates, ΔE^{Sub}, which are calculated using the following equations:

$$\Delta E^{\mathrm{Sub}} = E^{\mathrm{Sub}}_{Fr} - E^{\mathrm{Sub}} , \tag{4}$$

$$\Delta E^{\mathrm{Mol}} = E^{\mathrm{Mol}}_{Fr} - E^{\mathrm{Mol}} , \tag{5}$$

where E^{Mol} and E^{Sub} are the total energies of the isolated molecules and substrates optimized separately, while E^{Mol}_{Fr} and E^{Sub}_{Fr}, are obtained using the structure of molecule and substrate after the optimization with both systems interacting. As the molecules are adsorbed only on one side of the slab, the system becomes asymmetric. Thus, we have computed the adsorption energies with the inclusion of dipole corrections.[12] We show on Table S2 that the effect of adding the dipole correction for the computed adsorption energies was almost negligible; however, we emphasize that this computational artifact can significant change the computed work function and should be included when one is interested in such kind of property.

Table S2: Adsorption energies for different molecules on different adsorption sites with and without the inclusion of dipole corrections.

	Intermediate	E_{ad} (eV)	Dipole Corrected E_{ad} (eV)
$CN = 5$	COOH	−2.53	−2.53
	HCOO	−3.78	−3.79
	CO	−1.22	−1.22
	COH	−3.22	−3.21
	CHO	−1.99	−1.99
$CN = 7$	COOH	−2.30	−2.30
	HCOO	−3.40	−3.40
	CO	−1.13	−1.12
	COH	−3.14	−3.13
	CHO	−1.81	−1.81
$CN = 9$	COOH	−1.90	−1.90
	HCOO	−2.92	−2.92
	CO	−1.03	−1.03
	COH	−3.11	−3.11
	CHO	−1.55	−1.55

S5.1 COOH Adsorption

Figure S6 shows the distinct configurations obtained for COOH, while Table S3 shows energetic and structural properties for each configuration. After the geometry optimizations, in most cases COOH adsorbed with C and O interacting with the surface, with either the C−O or the C−OH bond parallel to the surface, with the former being energetically favorable. In some cases, we have observed a restructuring of the Cu_3/Cu(533) surface, which significantly lowers the adsorption energy due to a stabilization of the surface that can be observed in the negative sign of ΔE^{Sub}, or even the breaking of the COOH molecule into CO and OH fragments.

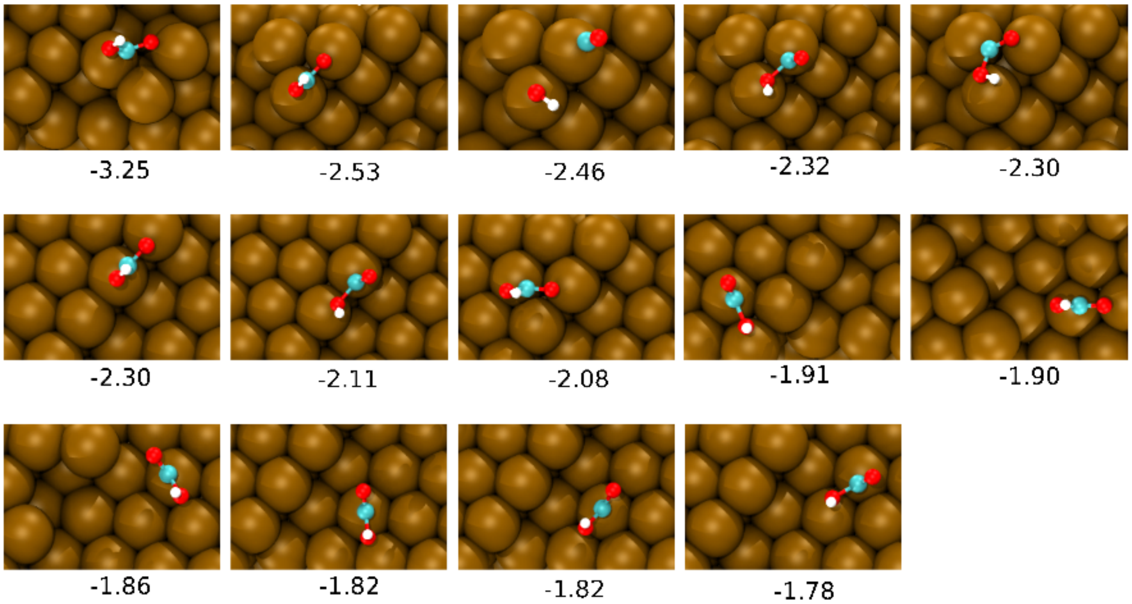

Figure S6: Distinct configurations for COOH interacting with Cu sites with different coordination together with their respective adsorption energies.

Table S3: Adsorption, interaction, and deformation energies in (eV), together with the shortest distance between the substrate and C and O atoms, C – O, C – OH, and O – H bond lengths, for COOH molecules interacting with different adsorption sites.

E_{ad} (eV)	E_{int} (eV)	ΔE^{Mol} (eV)	ΔE^{Sub} (eV)	C – Cu (Å)	O – Cu (Å)	C – O (Å)	C – OH (Å)	O – H (Å)
−3.25	−3.21	0.43	−0.47	1.96	1.98	1.27	1.35	0.99
−2.53	−3.03	0.40	0.11	1.93	2.00	1.27	1.34	0.99
−2.46	−4.31	1.80	0.05	1.84	1.82	1.14	NA	0.98
−2.32	−2.87	0.47	0.08	1.94	2.03	1.20	1.48	0.99
−2.30	−3.01	0.48	0.23	1.94	2.05	1.26	1.42	0.99
−2.30	−2.69	0.32	0.07	1.92	2.05	1.26	1.34	0.99
−2.11	−2.48	0.32	0.05	1.94	2.11	1.20	1.44	0.99
−2.08	−2.54	0.36	0.09	1.98	2.08	1.27	1.34	0.99
−1.91	−2.30	0.32	0.07	1.98	2.19	1.20	1.44	0.99
−1.90	−2.27	0.30	0.07	1.96	2.17	1.25	1.35	0.99
−1.82	−2.05	0.18	0.05	1.98	2.56	1.21	1.39	0.99
−1.82	−2.00	0.15	0.03	1.97	NA	1.22	1.37	0.99
−1.78	−2.04	0.20	0.05	1.99	2.45	1.21	1.40	0.99

S5.2 HCOO Adsorption

Figure S7 shows the distinct configurations obtained for HCOO, while Table S4 shows energetic and structural properties for each configuration. Differently from COOH, for HCOO, all the configurations were relatively similar, with the molecule binding through both O atoms, which reduced the number of obtained distinct configurations.

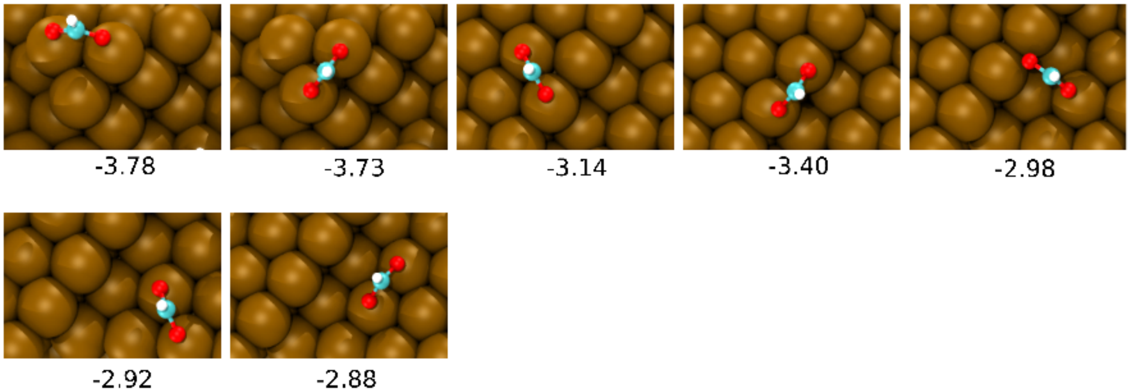

Figure S7: Distinct configurations for HCOO interacting with Cu sites with different coordination together with their respective adsorption energies.

Table S4: Adsorption, interaction, and deformation energies in (eV), together with the shortest distance between the substrate and O atoms, C−O, and C−H bond lengths, for HCOO molecules interacting with different adsorption sites.

E_{ad} (eV)	E_{int} (eV)	ΔE^{Mol} (eV)	ΔE^{Sub} (eV)	O−Cu$_{MIN}$ (Å)	C−O$_{MIN}$ (Å)	C−H (Å)
−3.78	−4.15	0.32	0.05	1.94	1.27	1.11
−3.73	−4.11	0.32	0.06	1.94	1.27	1.11
−3.40	−3.77	0.32	0.05	1.96	1.27	1.11
−3.14	−3.54	0.32	0.08	1.98	1.27	1.11
−2.98	−3.40	0.30	0.12	2.10	1.25	1.11
−2.92	−3.33	0.32	0.09	2.03	1.27	1.11
−2.88	−3.28	0.31	0.09	2.03	1.27	1.11

S5.3 CO Adsorption

Figure S8 shows the distinct configurations obtained for CO, while Table S5 shows energetic and structural properties for each configuration.

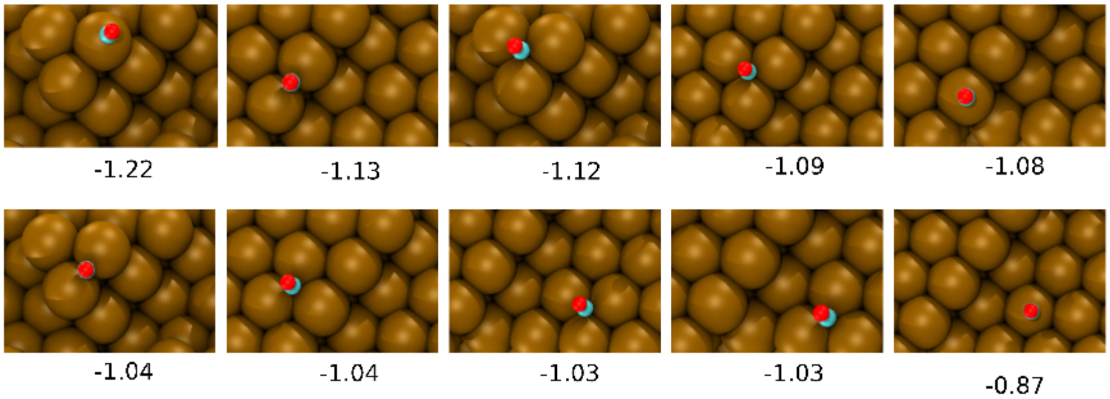

Figure S8: Distinct configurations for CO interacting with Cu sites with different coordination together with their respective adsorption energies.

Table S5: Adsorption, interaction, and deformation energies in (eV), shortest distance between the substrate and C atoms and C – O bond lengths for CO molecules interacting with different adsorption sites.

E_{ad} (eV)	E_{int} (eV)	ΔE^{Mol} (eV)	ΔE^{Sub} (eV)	C – Cu (Å)	C – O (Å)
−1.22	−1.25	0.01	0.02	1.82	1.15
−1.13	−1.21	0.04	0.05	1.97	1.17
−1.12	−1.26	0.11	0.04	2.02	1.18
−1.09	−1.21	0.09	0.04	2.02	1.18
−1.08	−1.11	0.01	0.03	1.84	1.15
−1.04	−1.14	0.05	0.04	1.96	1.17
−1.04	−1.16	0.08	0.03	2.04	1.18
−1.03	−1.16	0.08	0.04	2.03	1.18
−1.03	−1.15	0.08	0.04	2.03	1.18
−0.87	−0.91	0.01	0.03	1.85	1.15

S5.4 $C(OH)_2$ Adsorption

Figure S9 shows the distinct configurations obtained for $C(OH)_2$, while Table S6 shows energetic and structural properties for each configuration. For all cases, the adsorbate interacted with the surface through C atoms, and similarly to COOH, we observe restructuring of the Cu_3/Cu(533) surface.

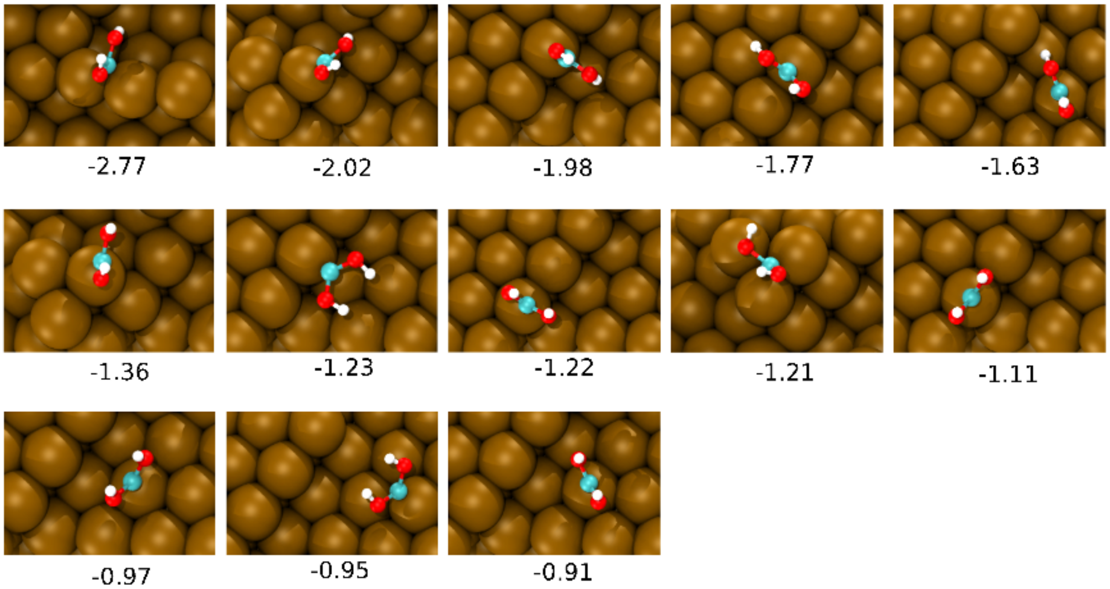

Figure S9: Distinct configurations for $C(OH)_2$ interacting with Cu sites with different coordination together with their respective adsorption energies.

Table S6: Adsorption, interaction, and deformation energies in (eV), shortest distance between the substrate and C atoms, C – OH, and O – H bond lengths for $C(OH)_2$ molecules interacting with different adsorption sites.

E_{ad} (eV)	E_{int} (eV)	ΔE^{Mol} (eV)	ΔE^{Sub} (eV)	C – Cu (Å)	C – OH$_{MIN}$ (Å)	O – H$_{MIN}$ (Å)
−2.77	−2.30	0.07	−0.55	2.01	1.34	0.98
−2.02	−2.15	0.09	0.03	1.90	1.32	0.99
−1.98	−2.10	0.09	0.03	1.92	1.32	0.99
−1.77	−1.87	0.06	0.04	1.91	1.32	0.99
−1.63	−1.81	0.09	0.09	1.95	1.32	0.99
−1.36	−1.68	0.29	0.03	1.88	1.33	0.99
−1.23	−1.62	0.33	0.06	1.93	1.33	0.99
−1.22	−1.55	0.29	0.03	1.90	1.33	0.99
−1.21	−2.32	1.00	0.11	1.97	1.37	0.98
−1.11	−1.44	0.29	0.05	1.91	1.33	0.99
−0.97	−1.34	0.29	0.07	1.93	1.33	0.99
−0.95	−1.38	0.33	0.10	1.94	1.33	0.99
−0.91	−1.29	0.29	0.09	1.94	1.33	0.99

S5.5 COH Adsorption

Figure S10 shows the distinct configurations obtained for COH, while Table S7 shows energetic and structural properties for each configuration. For all cases, the adsorbate interacted with the surface through C atoms positioned, in the majority of the cases, on hollow sites and with OH pointing away from the surface.

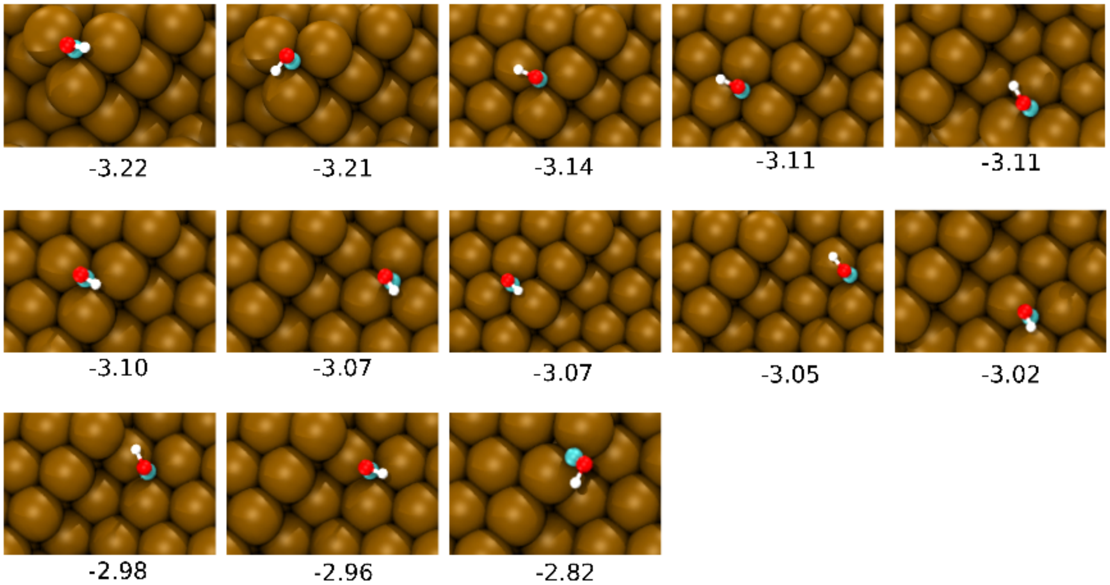

Figure S10: Distinct configurations for COH interacting with Cu sites with different coordination together with their respective adsorption energies.

Table S7: Adsorption, interaction, and deformation energies in (eV), shortest distance between the substrate and C atoms, C – OH, and O – H bond lengths for COH molecules interacting with different adsorption sites.

E_{ad} (eV)	E_{int} (eV)	ΔE^{Mol} (eV)	ΔE^{Sub} (eV)	C – Cu (Å)	C – OH (Å)	O – H (Å)
−3.22	−3.43	0.11	0.10	1.92	1.35	0.98
−3.21	−3.43	0.11	0.11	1.91	1.35	0.98
−3.14	−3.30	0.08	0.08	1.92	1.34	0.98
−3.11	−3.27	0.08	0.07	1.90	1.34	0.98
−3.11	−3.25	0.07	0.07	1.90	1.33	0.98
−3.10	−3.28	0.09	0.09	1.92	1.34	0.98
−3.07	−3.22	0.08	0.08	1.91	1.33	0.98
−3.07	−3.24	0.09	0.09	1.90	1.34	0.98
−3.05	−3.21	0.07	0.09	1.91	1.33	0.98
−3.02	−3.18	0.08	0.08	1.91	1.33	0.98
−2.98	−3.13	0.06	0.08	1.90	1.33	0.99
−2.96	−3.12	0.09	0.07	1.92	1.34	0.98
−2.92	−2.92	0.03	0.07	1.87	1.31	0.98

S5.6 CHO Adsorption

Figure S11 shows the distinct configurations obtained for CHO, while Table S8 shows energetic and structural properties for each configuration. For most cases, the adsorbate interacted with the surface through C and O atoms. We also observed some cases where the adsorbate interacted via the C atoms, with these configurations being higher in energy. For these adsorbates, we also observe restructuring of the Cu_3/Cu(533) surface.

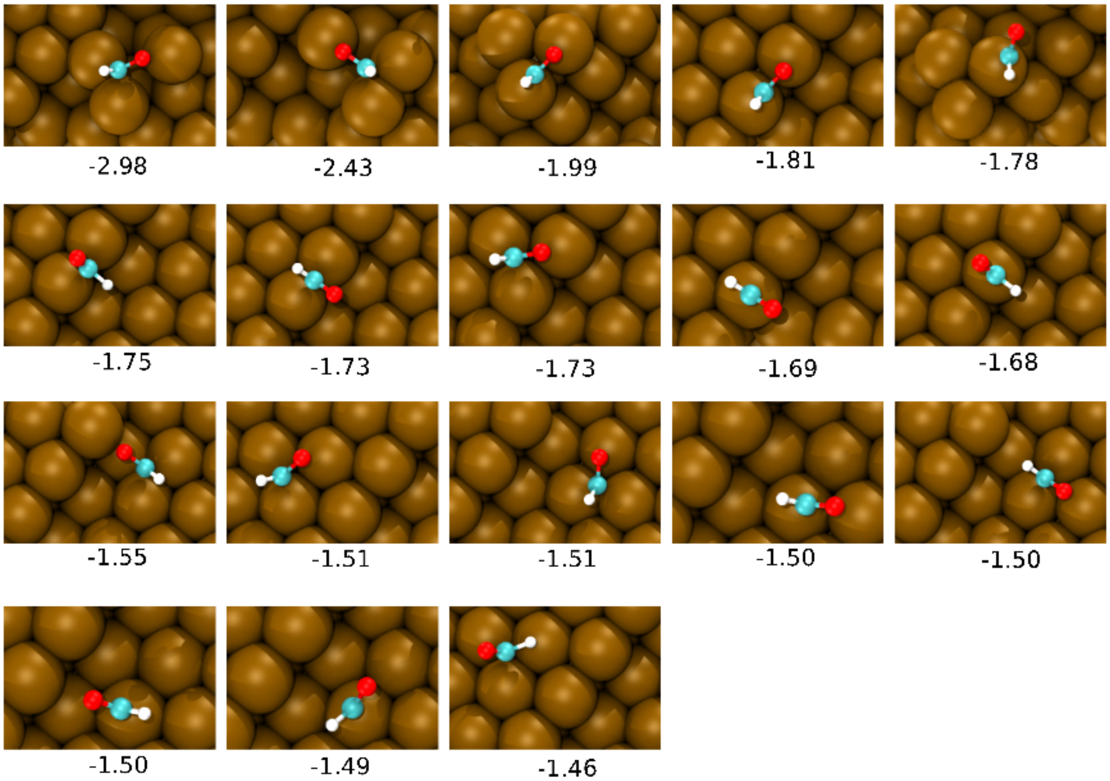
-2.98
-2.43
-1.99
-1.81
-1.78
-1.75
-1.73
-1.73
-1.69
-1.68
-1.55
-1.51
-1.51
-1.50
-1.50
-1.50
-1.49
-1.46

Figure S11: CHO interacting with Cu sites with different coordinations together with their respective adsorption energies.

Table S8: Adsorption, interaction, and deformation energies in (eV), shortest distance between the substrate and C and O atoms, C−O, and C−H bond lengths for CHO molecules interacting with different adsorption sites.

E_{ad} (eV)	E_{int} (eV)	ΔE^{Mol} (eV)	ΔE^{Sub} (eV)	C−Cu (Å)	O−Cu (Å)	C−O (Å)	C−H_{MIN} (Å)
−2.98	−3.00	0.35	−0.32	2.04	1.95	1.27	1.12
−2.43	−2.88	0.34	0.11	2.04	1.95	1.27	1.12
−1.99	−2.34	0.25	0.11	1.92	2.02	1.26	1.12
−1.81	−2.06	0.19	0.06	1.92	2.07	1.25	1.12
−1.78	−1.84	0.04	0.02	1.92	NA	1.21	1.13
−1.75	−1.83	0.05	0.03	2.06	NA	1.22	1.13
−1.73	−1.84	0.07	0.04	2.08	NA	1.22	1.12
−1.73	−2.16	0.31	0.12	2.05	2.05	1.27	1.11
−1.69	−1.74	0.03	0.02	1.95	NA	1.21	1.12
−1.68	−1.72	0.02	0.01	1.94	NA	1.20	1.13
−1.55	−1.99	0.28	0.16	2.12	2.09	1.26	1.12
−1.51	−1.74	0.18	0.05	1.98	2.24	1.25	1.12
−1.51	−1.80	0.21	0.08	2.05	2.19	1.25	1.12
−1.50	−1.68	0.13	0.05	1.94	2.25	1.24	1.12
−1.50	−1.79	0.21	0.08	2.05	2.18	1.25	1.12
−1.50	−1.60	0.05	0.06	1.98	NA	1.21	1.12
−1.49	−1.56	0.03	0.04	1.98	NA	1.21	1.12
−1.46	−1.64	0.15	0.04	2.10	NA	1.22	1.20

S5.7 C Adsorption

Figure S12 shows the distinct configurations obtained for C interacting with Cu surfaces, while Table S9 shows energetic and structural properties for each configuration. For most cases, C adsorbed on hollow sites, causing significant deformations for the surfaces when adsorbed on low-coordinated sites, which can be observed by the magnitude of ΔE^{Mol} .

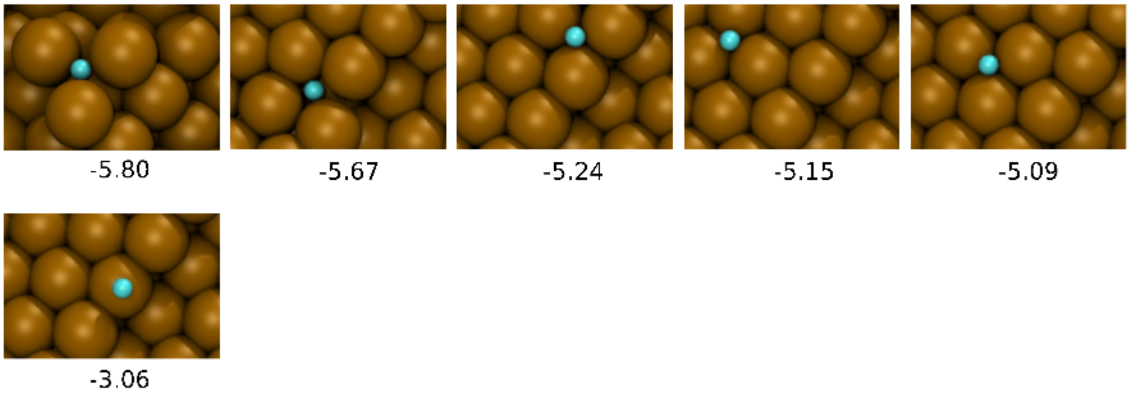

Figure S12: C interacting with Cu sites with different coordination together with their respective adsorption energies.

Table S9: Adsorption, interaction, and deformation energies in (eV) and shortest distance between the substrate and C atoms for C atoms interacting with different adsorption sites.

E_{ad} (eV)	E$_{int}$ (eV)	ΔE^{Sub} (eV)	C−Cu (Å)
−5.80	−6.32	0.53	1.86
−5.67	−6.48	0.91	1.85
−5.24	−5.48	0.24	1.83
−5.15	−5.28	0.13	1.83
−5.09	−5.24	0.16	1.83
−3.06	−3.14	0.08	1.72

S5.8 CHOH Adsorption

Figure S13 shows the distinct configurations obtained for CHOH interacting with Cu surfaces, while Table S10 shows energetic and structural properties for each configuration. For most cases, CHOH adsorbed via C atoms, with the preferred adsorption site changing with the coordination of adsorption sites on each region. Again, surface restructuring was observed for low-coordinated sites.

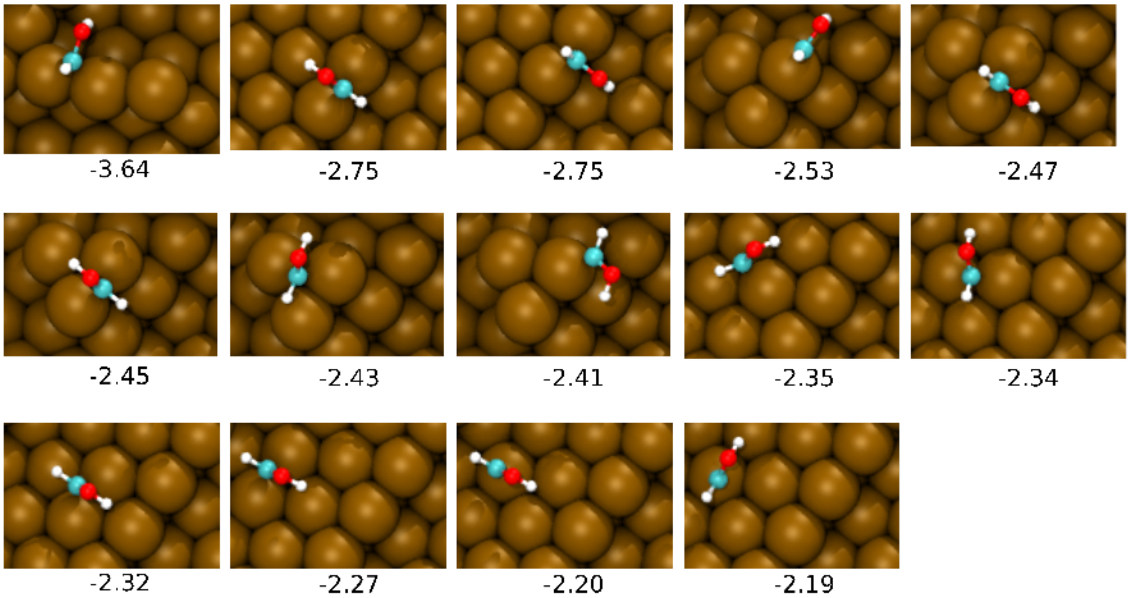
-3.64 -2.75 -2.75 -2.53 -2.47
-2.45 -2.43 -2.41 -2.35 -2.34
-2.32 -2.27 -2.20 -2.19

Figure S13: CHOH interacting with Cu sites with different coordination together with their respective adsorption energies.

Table S10: Adsorption, interaction, and deformation energies in (eV)**, shortest distance between the substrate and C atoms, C – O, C – H, and O – H bond lengths for CHOH molecules interacting with different adsorption sites.**

E_{ad} (eV)	E$_{int}$ (eV)	ΔE^{Mol} (eV)	ΔE^{Sub} (eV)	C – Cu (Å)	C – O (Å)	C – H (Å)	O – H (Å)
−3.64	−3.17	0.07	−0.55	1.97	1.36	1.10	0.99
−2.75	−2.87	0.07	0.06	1.99	1.35	1.10	0.98
−2.75	−2.87	0.06	0.06	2.00	1.34	1.10	1.00
−2.53	−2.59	0.04	0.02	1.86	1.31	1.11	1.01
−2.47	−2.60	0.08	0.04	1.99	1.37	1.10	0.98
−2.45	−2.60	0.10	0.05	1.98	1.37	1.10	0.98
−2.43	−2.61	0.10	0.08	2.00	1.39	1.13	0.98
−2.41	−2.48	0.05	0.02	1.86	1.34	1.11	0.98
−2.35	−2.49	0.06	0.07	2.01	1.36	1.11	0.98
−2.34	−2.50	0.06	0.11	2.01	1.35	1.10	0.99
−2.32	−2.44	0.06	0.07	2.03	1.36	1.11	0.98
−2.27	−2.44	0.06	0.11	2.01	1.35	1.11	0.99
−2.20	−2.30	0.06	0.04	1.88	1.32	1.11	0.99
−2.19	−2.27	0.04	0.04	1.90	1.33	1.10	0.99

S5.9 CH_2O Adsorption

Figure S14 shows the distinct configurations obtained for CH_2O interacting with Cu surfaces, while Table S11 shows energetic and structural properties for each configuration.

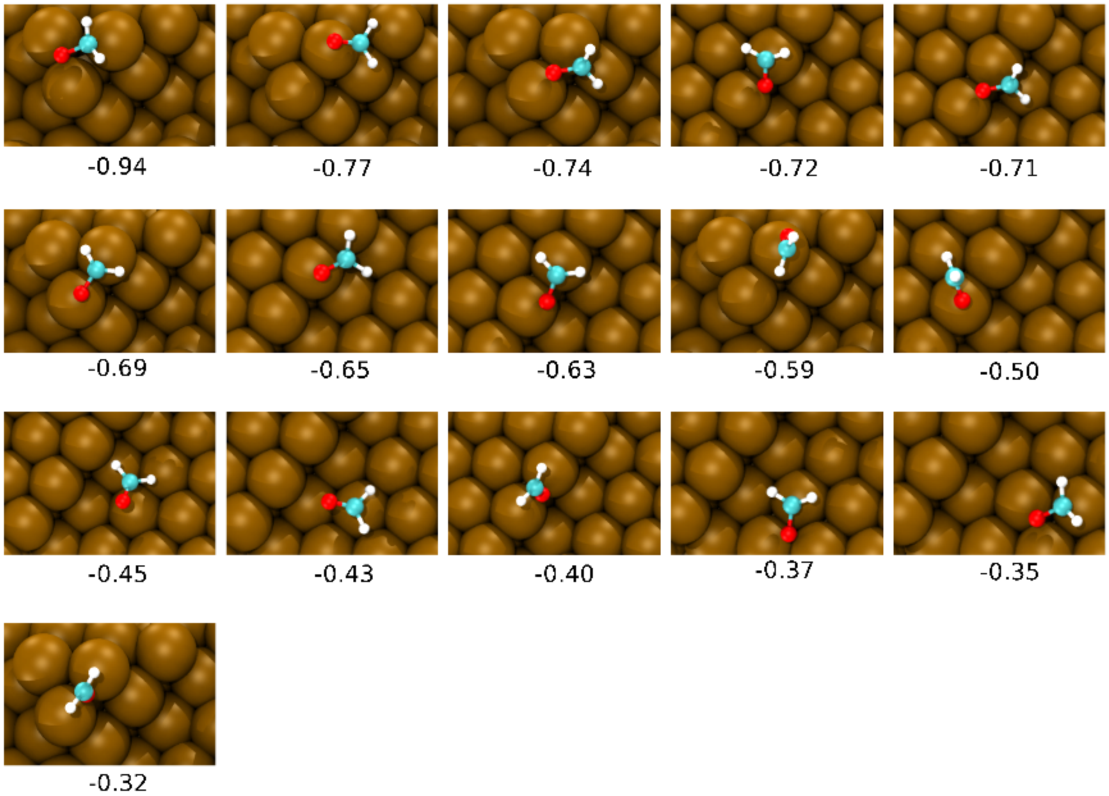

Figure S14: CH_2O interacting with Cu sites with different coordination together with their respective adsorption energies.

Table S11: Adsorption, interaction, and deformation energies in (eV), shortest distance between the substrate and C and O atoms, C – O, and C – H bond lengths for CH_2O molecules interacting with different adsorption sites.

E_{ad} (eV)	E_{int} (eV)	ΔE^{Mol} (eV)	ΔE^{Sub} (eV)	C – Cu (Å)	O – Cu (Å)	C – O (Å)	C – H_{MIN} (Å)
−0.94	−2.62	1.44	0.24	2.00	1.99	1.39	1.10
−0.77	−0.99	0.21	0.02	2.11	1.96	1.28	1.11
−0.74	−1.33	0.54	0.05	2.05	2.00	1.32	1.10
−0.72	−1.23	0.45	0.06	2.06	2.02	1.31	1.10
−0.71	−1.18	0.35	0.05	2.09	2.05	1.30	1.10
−0.69	−1.28	0.55	0.03	2.11	1.91	1.31	1.11
−0.65	−0.95	0.28	0.03	2.25	1.98	1.28	1.11
−0.63	−1.03	0.36	0.04	2.14	1.97	1.29	1.11
−0.59	−0.63	0.03	0.02	1.97	2.92	1.23	1.11
−0.50	−0.55	0.02	0.03	2.96	2.13	1.23	1.11
−0.45	−0.45	0.01	0.00	3.25	3.61	1.21	1.12
−0.43	−0.43	0.00	0.00	3.00	2.54	1.21	1.12
−0.40	−0.46	0.05	0.02	2.15	3.10	1.24	1.10
−0.37	−1.08	0.64	0.07	2.11	2.11	1.32	1.10
−0.35	−1.16	0.73	0.08	2.10	2.11	1.33	1.10
−0.32	−0.43	0.08	0.03	2.11	3.19	1.25	1.10

S5.10 CH Adsorption

Figure S15 shows the distinct configurations obtained for CH interacting with Cu surfaces, while Table S12 shows energetic and structural properties for each configuration.

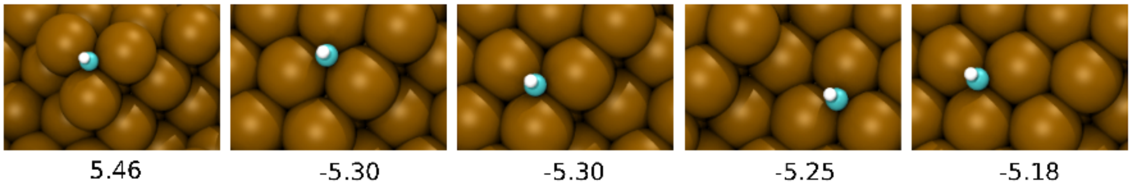

Figure S15: CH interacting with Cu sites with different coordination together with their respective adsorption energies.

Table S12: Adsorption, interaction, and deformation energies in (eV), shortest distance between the substrate and C and C – H bond lengths for CH molecules interacting with different adsorption sites.

E_{ad} (eV)	E_{int} (eV)	ΔE^{Mol} (eV)	ΔE^{Sub} (eV)	C – Cu (Å)	C – H (Å)
−5.46	−5.63	0.02	0.15	1.89	1.10
−5.30	−5.43	0.03	0.10	1.89	1.10
−5.30	−5.43	0.03	0.10	1.89	1.10
−5.25	−5.36	0.03	0.08	1.90	1.10
−5.18	−5.30	0.03	0.10	1.90	1.10

S5.11 CH_2OH Adsorption

Figure S16 shows the distinct configurations obtained for CH_2OH interacting with Cu surfaces, while Table S13 shows energetic and structural properties for each configuration. In all the coordination regions, configurations where CH_2OH adsorbs via C or C and O atoms are close in energy. Although the difference in energy between these distinct configurations is too small to generate significant changes in our analysis, it could be interesting to explore if they could impact calculated kinetic parameters.

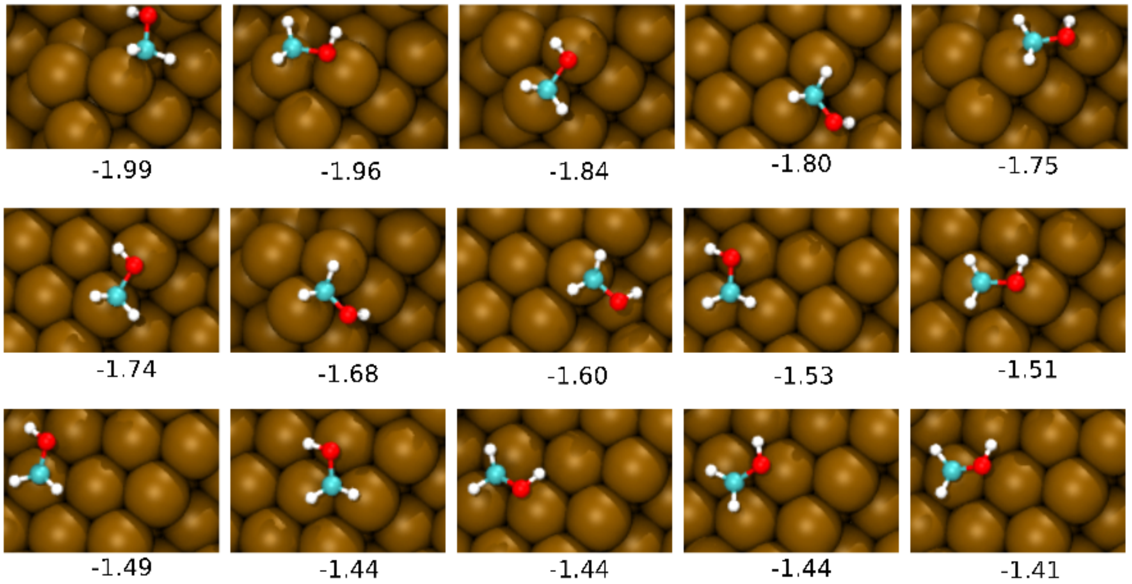

Figure S16: CH_2OH interacting with Cu sites with different coordination together with their respective adsorption energies.

Table S13: Adsorption, interaction, and deformation energies in (eV), together with shortest distance between the substrate and C and O atoms, C−O, C−H, and O−H bond lengths for CH_2OH molecules interacting with different adsorption sites.

E_{ad} (eV)	E_{int} (eV)	ΔE^{Mol} (eV)	ΔE^{Sub} (eV)	C−Cu (Å)	O−Cu (Å)	C−O (Å)	C−H_{MIN} (Å)	O−H (Å)
−1.99	−2.75	0.60	0.16	1.99	2.16	1.48	1.10	0.98
−1.96	−2.62	0.61	0.04	1.96	2.03	1.50	1.10	0.97
−1.84	−2.42	0.53	0.05	1.96	2.05	1.50	1.10	0.97
−1.80	−2.18	0.35	0.04	2.08	2.74	1.41	1.10	0.98
−1.75	−1.92	0.14	0.02	1.97	2.82	1.41	1.10	0.99
−1.74	−2.11	0.34	0.04	1.97	2.12	1.48	1.10	0.98
−1.68	−2.14	0.42	0.04	2.08	2.80	1.43	1.10	0.98
−1.60	−1.78	0.16	0.02	2.00	2.76	1.40	1.10	0.98
−1.53	−1.87	0.28	0.06	2.13	2.30	1.44	1.10	0.99
−1.51	−1.94	0.36	0.07	2.02	2.17	1.47	1.10	0.98
−1.49	−1.68	0.14	0.04	2.05	2.75	1.41	1.09	0.99
−1.44	−1.84	0.34	0.06	2.16	2.39	1.45	1.10	0.98
−1.44	−1.79	0.29	0.06	2.12	2.41	1.44	1.10	0.98
−1.44	−1.79	0.30	0.06	2.15	2.38	1.44	1.10	0.98
−1.41	−1.60	0.14	0.05	2.05	2.77	1.41	1.10	0.98

S5.12 CH_3O Adsorption

Figure S17 shows the distinct configurations obtained for CH_3O interacting with Cu surfaces, while Table S14 shows energetic and structural properties for each configuration.

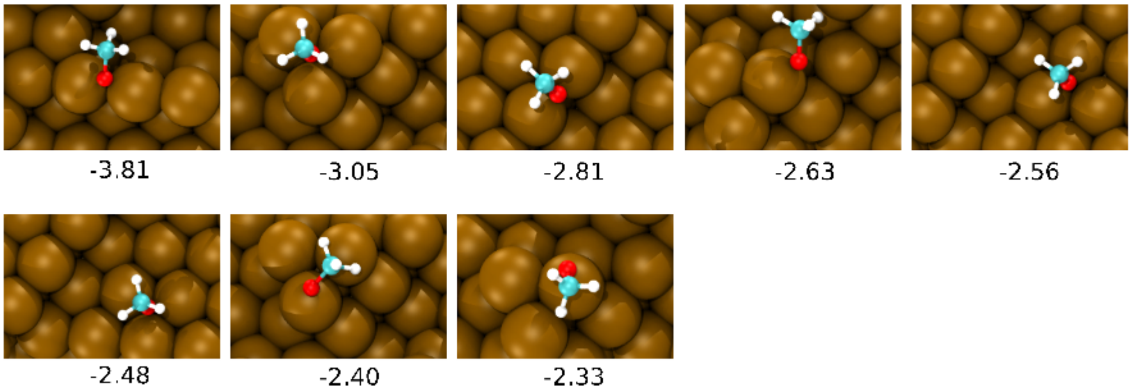

Figure S17: CH_3O interacting with Cu sites with different coordination together with their respective adsorption energies.

Table S14: Adsorption, interaction, and deformation energies in (eV), shortest distance between the substrate and O atoms, C−O, and C−H bond lengths for CH_3O molecules interacting with different adsorption sites.

E_{ad} (eV)	E_{int} (eV)	ΔE^{Mol} (eV)	ΔE^{Sub} (eV)	O−Cu (Å)	C−O (Å)	$C-H_{MIN}$ (Å)
−3.81	−3.37	0.10	−0.54	1.92	1.43	1.10
−3.05	−3.26	0.12	0.09	2.03	1.43	1.10
−2.81	−2.98	0.10	0.07	1.94	1.43	1.10
−2.63	−2.72	0.06	0.04	1.84	1.37	1.11
−2.56	−2.77	0.10	0.11	2.02	1.43	1.10
−2.48	−2.68	0.10	0.09	2.04	1.43	1.10
−2.40	−2.55	0.08	0.06	1.86	1.39	1.11
−2.33	−2.42	0.07	0.02	1.81	1.41	1.10

S5.13 CH_2 Adsorption

Figure S18 shows the distinct configurations obtained for CH_2 interacting with Cu surfaces, while Table S15 shows energetic and structural properties for each configuration.

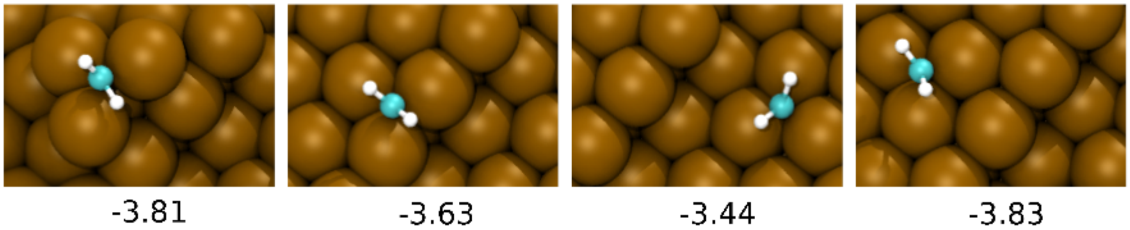

Figure S18: CH_2 interacting with Cu sites with different coordination together with their respective adsorption energies.

Table S15: Adsorption, interaction, and deformation energies in (eV), shortest distance between the substrate and C atoms and C−H bond lengths for CH_2 molecules interacting with different adsorption sites.

E_{ad} (eV)	E_{int} (eV)	ΔE^{Mol} (eV)	ΔE^{Sub} (eV)	C−Cu (Å)	$C-H_{MIN}$ (Å)
−3.81	−4.39	0.36	0.22	1.97	1.10
−3.63	−4.03	0.35	0.05	1.96	1.10
−3.44	−3.88	0.37	0.07	1.97	1.10
−3.38	−3.82	0.37	0.07	1.97	1.10

S5.14 O Adsorption

Figure S19 shows the distinct configurations obtained for O interacting with Cu surfaces, while Table S16 shows energetic and structural properties for each configuration.

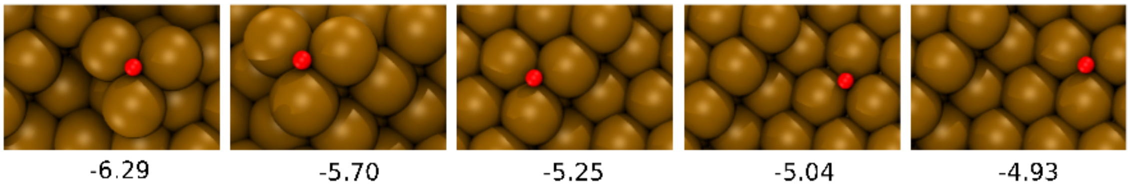

Figure S19: O interacting with Cu sites with different coordination together with their respective adsorption energies.

Table S16: Adsorption, interaction, and deformation energies in (eV)**, together with the shortest distance between the substrate and O atoms for O interacting with different adsorption sites.**

E_{ad} (eV)	E_{int} (eV)	ΔE^{Sub} (eV)	O – Cu (Å)
−6.29	−5.89	−0.41	1.88
−5.70	−5.80	0.10	1.88
−5.25	−5.37	0.12	1.87
−5.04	−5.19	0.14	1.89
−4.93	−5.07	0.14	1.89

S5.15 CH_3 Adsorption

Figure S20 shows the distinct configurations obtained for CH_3 interacting with Cu surfaces, while Table S17 shows energetic and structural properties for each configuration.

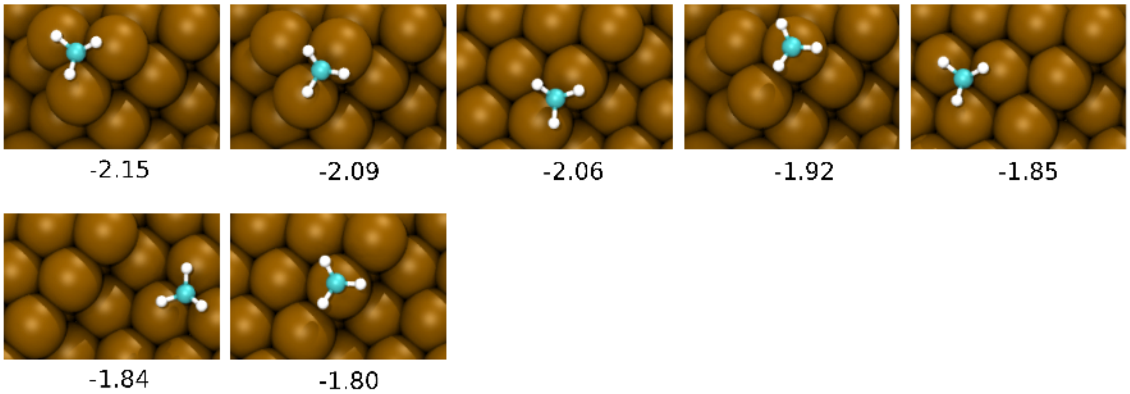

-2.15 -2.09 -2.06 -1.92 -1.85

-1.84 -1.80

Figure S20: CH_3 interacting with Cu sites with different coordination together with their respective adsorption energies.

Table S17: Adsorption, interaction, and deformation energies in (eV), shortest distance between the substrate and C and C – H bond lengths for CH_3 molecules interacting with different adsorption sites.

E_{ad} (eV)	E_{int} (eV)	ΔE^{Mol} (eV)	ΔE^{Sub} (eV)	C – Cu (Å)	C – H_{MIN} (Å)
−2.15	−2.71	0.53	0.03	2.15	1.11
−2.10	−2.61	0.47	0.04	2.06	1.10
−2.06	−2.53	0.42	0.04	2.08	1.10
−1.92	−2.24	0.30	0.03	1.94	1.10
−1.85	−2.32	0.44	0.04	2.22	1.10
−1.84	−2.33	0.44	0.04	2.21	1.10
−1.80	−2.11	0.29	0.02	1.97	1.10

S5.16 OH Adsorption

Figure S21 shows the distinct configurations obtained for OH interacting with Cu surface, while Table S18 shows energetic and structural properties for each configuration.

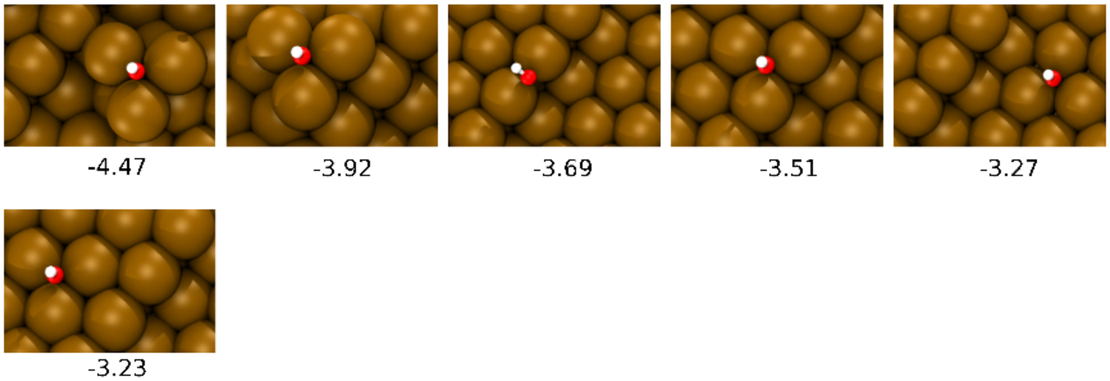

Figure S21: OH interacting with Cu sites with different coordination together with their respective adsorption energies.

Table S18: Adsorption, interaction, and deformation energies in (eV)**, shortest distance between the substrate and O atoms and O – H bond lengths for OH molecules interacting with different adsorption sites.**

E_{ad} (eV)	E$_{int}$ (eV)	ΔE^{Mol} (eV)	ΔE^{Sub} (eV)	O – Cu (Å)	O – H (Å)
−4.47	−4.12	0.00	−0.35	2.02	0.97
−3.92	−4.01	0.00	0.09	2.02	0.97
−3.69	−3.77	0.00	0.08	1.95	0.97
−3.51	−3.62	0.00	0.11	1.98	0.97
−3.27	−3.40	0.00	0.13	2.02	0.97
−3.23	−3.34	0.00	0.10	2.03	0.97

S5.17 H Adsorption

Figure S22 shows the distinct configurations obtained for H interacting with Cu surface, while Table S19 shows energetic and structural properties for each configuration.

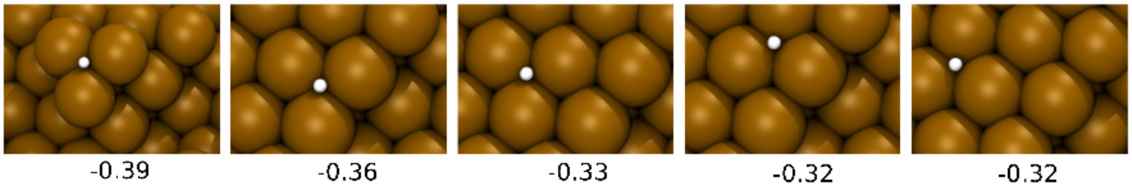

Figure S22: H interacting with Cu sites with different coordination together with their respective adsorption energies.

Table S19: Adsorption, interaction, and deformation energies in (eV), together with the shortest distance between the substrate and H atoms for H interacting with different adsorption sites.

E_{ad} (eV)	E_{int} (eV)	ΔE^{Sub} (eV)	H−Cu (Å)
−0.39	−0.42	0.03	1.75
−0.36	−0.38	0.02	1.73
−0.33	−0.36	0.03	1.73
−0.32	−0.35	0.03	1.75
−0.32	−0.34	0.02	1.72

S6 Energetic Contributions from Vibrational Calculations

In the main text, we present the average values and the standard deviations of $(ZPE + \int C_p dT - TS)$ for each adsorbate, which were used to construct the reaction energy diagrams. Meanwhile, Table S20 show the values for these terms calculated for each adsorbate on the different coordination regions.

Table S20: Calculated $ZPE+\int C_p dT - TS$ for all adsorbates in the three coordination regions.

	$CN=9$			$CN=7$			$CN=5$		
	ZPE	$\int C_p dT$	TS	ZPE	$\int C_p dT$	TS	ZPE	$\int C_p dT$	TS
COOH	0.60	0.11	0.24	0.62	0.12	0.23	0.61	0.10	0.20
HCOO	0.62	0.10	0.20	0.63	0.10	0.20	0.63	0.10	0.18
CO	0.18	0.08	0.14	0.19	0.08	0.18	0.19	0.08	0.18
$C(OH)_2$	0.89	0.11	0.24	0.91	0.11	0.24	0.90	0.11	0.24
COH	0.47	0.08	0.13	0.46	0.08	0.15	0.47	0.08	0.14
CHO	0.47	0.07	0.14	0.46	0.08	0.17	0.47	0.07	0.14
OCH_2	0.71	0.12	0.35	0.77	0.09	0.16	0.77	0.07	0.12
CHOH	0.76	0.09	0.19	0.78	0.09	0.18	0.76	0.09	0.25
C	0.10	0.04	0.06	0.09	0.02	0.03	0.09	0.02	0.03
OCH_3	1.10	0.10	0.19	1.10	0.10	0.21	1.10	0.10	0.19
CH_2OH	1.06	0.10	0.18	1.14	0.10	0.19	1.07	0.09	0.17
CH	0.35	0.03	0.04	0.35	0.03	0.04	0.34	0.03	0.05
O	0.07	0.03	0.04	0.07	0.03	0.04	0.07	0.03	0.04
CH_2	0.59	0.06	0.10	0.59	0.06	0.09	0.59	0.05	0.08
OH	0.34	0.05	0.08	0.35	0.05	0.09	0.34	0.05	0.08
CH_3	0.91	0.07	0.12	0.91	0.08	0.16	0.89	0.08	0.13
H	0.17	0.00	0.01	0.17	0.01	0.01	0.16	0.01	0.01

For the non-adsorbed species, the zero point energies, enthalpic temperature and entropy corrections were calculated in the ideal-gas limit using the thermochemistry model from the atomic simulation environment.[13] To allow a direct comparison, we have considered the same values of fugacities using the assumptions that are widely employed in the literature, e.g, gaseous products are calculated at partial pressures related to the Faradaic yields obtained experimentally by Hori *et al.*[14] converted to molar yields, while water and liquid products are calculated with values of fugacities that correspond to vapor-liquid equilibrium, considering products at a liquid mole fractions of 0.01.[15–18] To account for the inconsistency of thermochemical data calculated with the PBE functional, an additional −0.51 eV was added as a gas-phase correction (GPC) to the energy of CO as calculated by Peterson *et al.*.[15]

Table S21: Averages and standard deviations of $ZPE + \int C_p dT - TS$ and gas-phase correction values for all non-adsorbed species, together with the assumed fugacities obtained by Peterson *et al.*.[15]

	Fugacity (Pa)	ZPE (eV)	$\int C_p dT$ (eV)	TS (eV)	GPC (eV)
CO_2	101325	0.31	0.10	0.66	
CO	5562	0.13	0.10	0.67	−0.51
HCOOH	2	0.89	0.11	1.04	
H_2	30296	0.27	0.09	0.43	
CH_4	20467	1.19	0.10	0.62	
CH_3OH	6079	1.36	0.12	0.81	
H_2O	3534	0.56	0.10	0.67	

S7 Example of Reaction Free Energies Diagram Determination

Figure S23 shows an example of free energy diagrams towards a) HCOOH and b) CO.

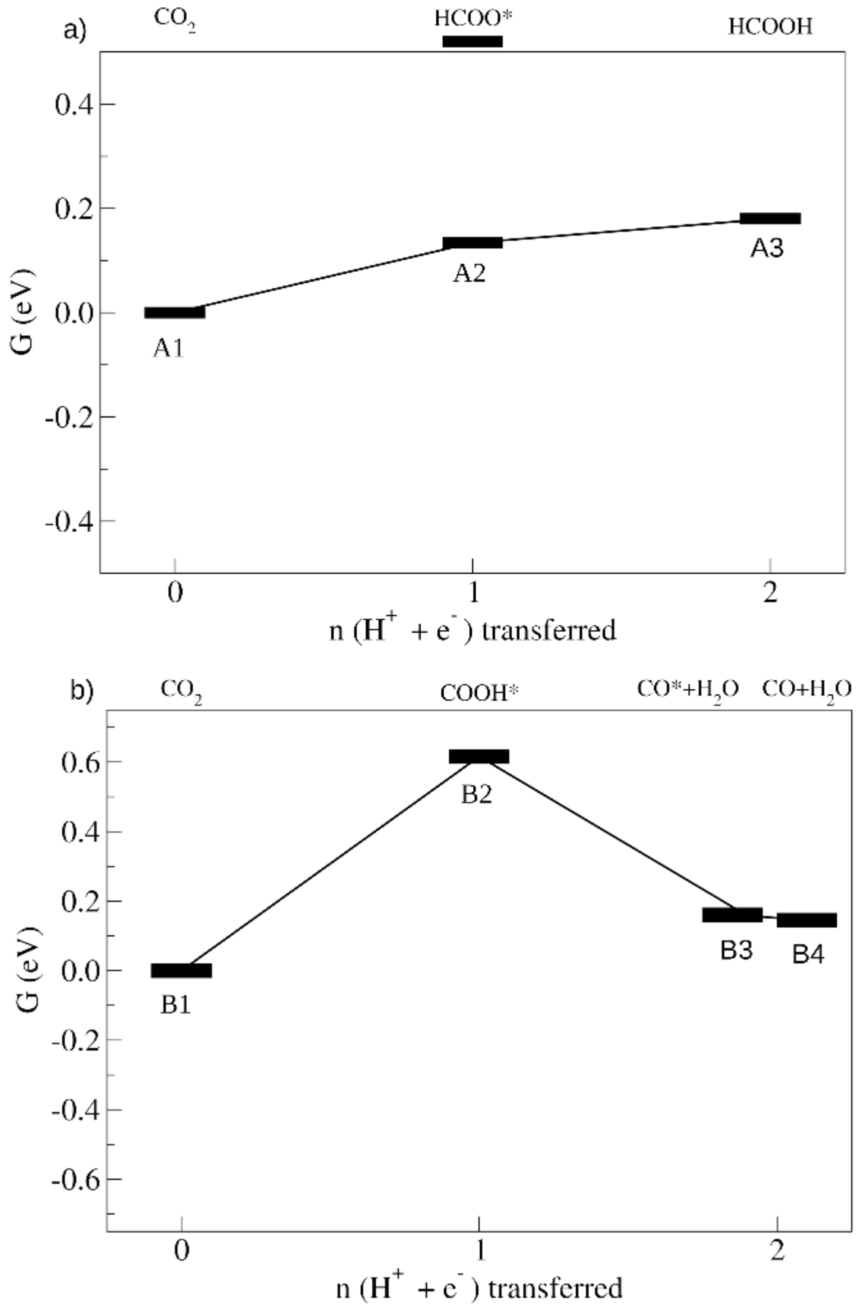

Figure S23: Example of free energy diagrams for CO_2 reduction towards a) HCOOH and b) CO. Solvation energies for the diagrams were obtained from the work of Peterson *et al.*.[15]

The diagrams were constructed calculating the free energy change for each reaction step. For example, for HCOOH formation the free energy changes for each reaction step was defined as follows:

$$\Delta G(A2 - A1) = (G_{\mathrm{HCOO^*}} + 0.5G_{\mathrm{H_2}}) - (G_{\mathrm{CO_2}} + G_{\mathrm{H_2}} + G_{Sub}) \; ; \qquad (6)$$

$$\Delta G(A3 - A2) = (G_{\mathrm{HCOOH}} + G_{Sub}) - (G_{\mathrm{HCOO^*}} + 0.5G_{\mathrm{H_2}}); \tag{7}$$

where, $G_{\mathrm{HCOO^*}}$ represents the free energy for adsorbed HCOO, while $G_{\mathrm{CO_2}}$ and G_{Sub} represents the free energies of CO_2 and the Cu surface calculated separately.

Similarly, for CO formation the free energy changes for each reaction step are calculated as follows:

$$\Delta G(B2 - B1) = (G_{\mathrm{COOH^*}} + 0.5G_{\mathrm{H_2}}) - (G_{\mathrm{CO_2}} + G_{\mathrm{H_2}} + G_{Sub}); \tag{8}$$

$$\Delta G(B3 - B2) = (G_{\mathrm{CO^*}} + G_{\mathrm{H_2O}}) - (G_{\mathrm{COOH^*}} + 0.5G_{\mathrm{H_2}}); \tag{9}$$

$$\Delta G(B4 - B3) = (G_{\mathrm{CO}} + G_{\mathrm{H_2O}} + G_{Sub}) - (G_{\mathrm{CO^*}} + G_{\mathrm{H_2O}}); \tag{10}$$

The same procedure was used for all the other reactions, where the free energy of the CO_2 molecule, Cu surface, and the number of proton-coupled electrons necessary to complete the reaction was always used as reference.

S8 Reaction Free Energies for CO_2 Reduction towards CO, HCOOH, CH_3OH, and CH_4

In the manuscript, we have presented reaction free energy diagrams calculated for $U = 0$ (V vs RHE). Using this analysis, we determined the potential-determining reaction step for each reaction on the different coordination regions, and determined possible reaction mechanisms under thermodynamic arguments. Here, we show the same free energy diagrams but calculated for the electrode potential required to allow each reaction. The diagrams illustrated in Figures S24, S26, and S28 were obtained with the solvation scheme referred as SC1 in the manuscript[15], while the diagrams in Figures S25, S27, and S29 were obtained with the solvation scheme referred as SC2 in the manuscript[19].

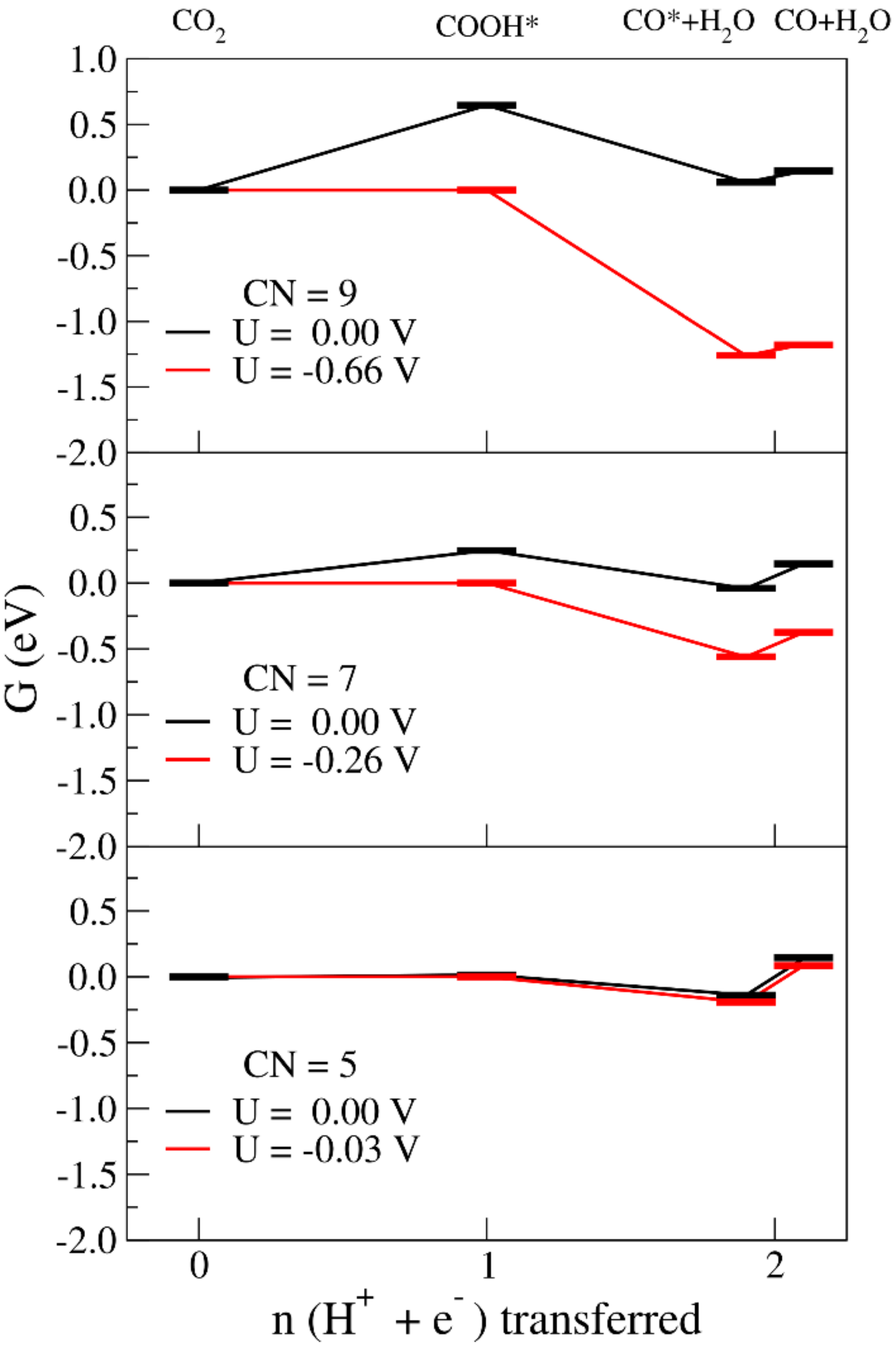

Figure S24: Free energy diagrams for CO_2 reduction towards CO on regions with different levels of coordination. Black curves represent diagrams obtained for $U = 0$ (V vs RHE) while red curves represent the same diagrams calculated for the electrode potential required to allow each reaction. Solvation energies for this diagram were obtained from the work of Peterson *et al.*.[15] The reaction path with the lowest theoretical onset potential is connected with straight lines and for possible bifurcating reaction paths, the intermediates are indicated with different symbols.

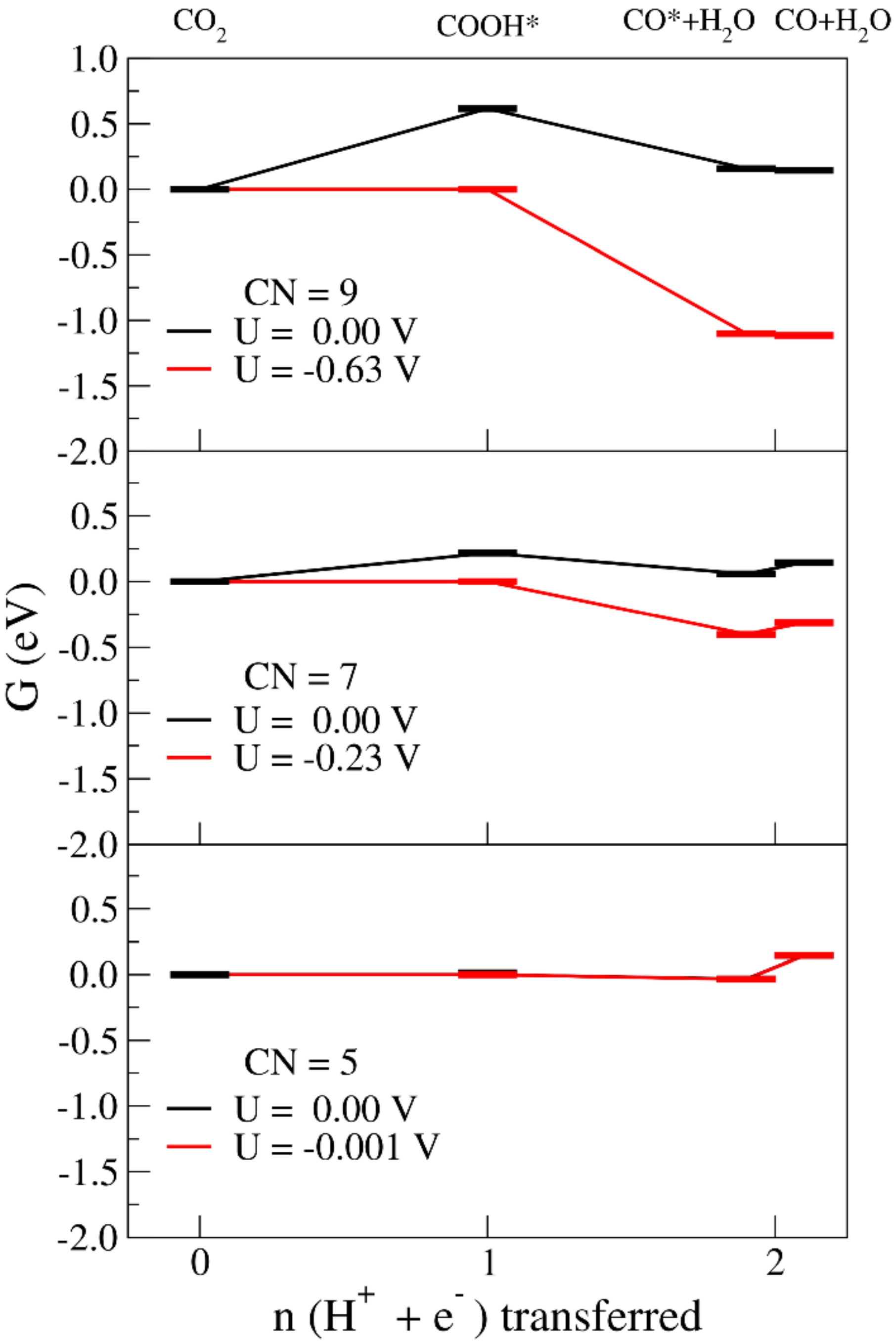

Figure S25: Free energy diagrams for CO_2 reduction towards CO on regions with different levels of coordination. Black curves represent diagrams obtained for $U = 0$ (V vs RHE) while red curves represent the same diagrams calculated for the electrode potential required to allow each reaction. Solvation energies for this diagram were obtained from the work of Rendón-Calle *et al.*.[19] The reaction path with the lowest theoretical onset potential is connected with straight lines and for possible bifurcating reaction paths, the intermediates are indicated with different symbols.

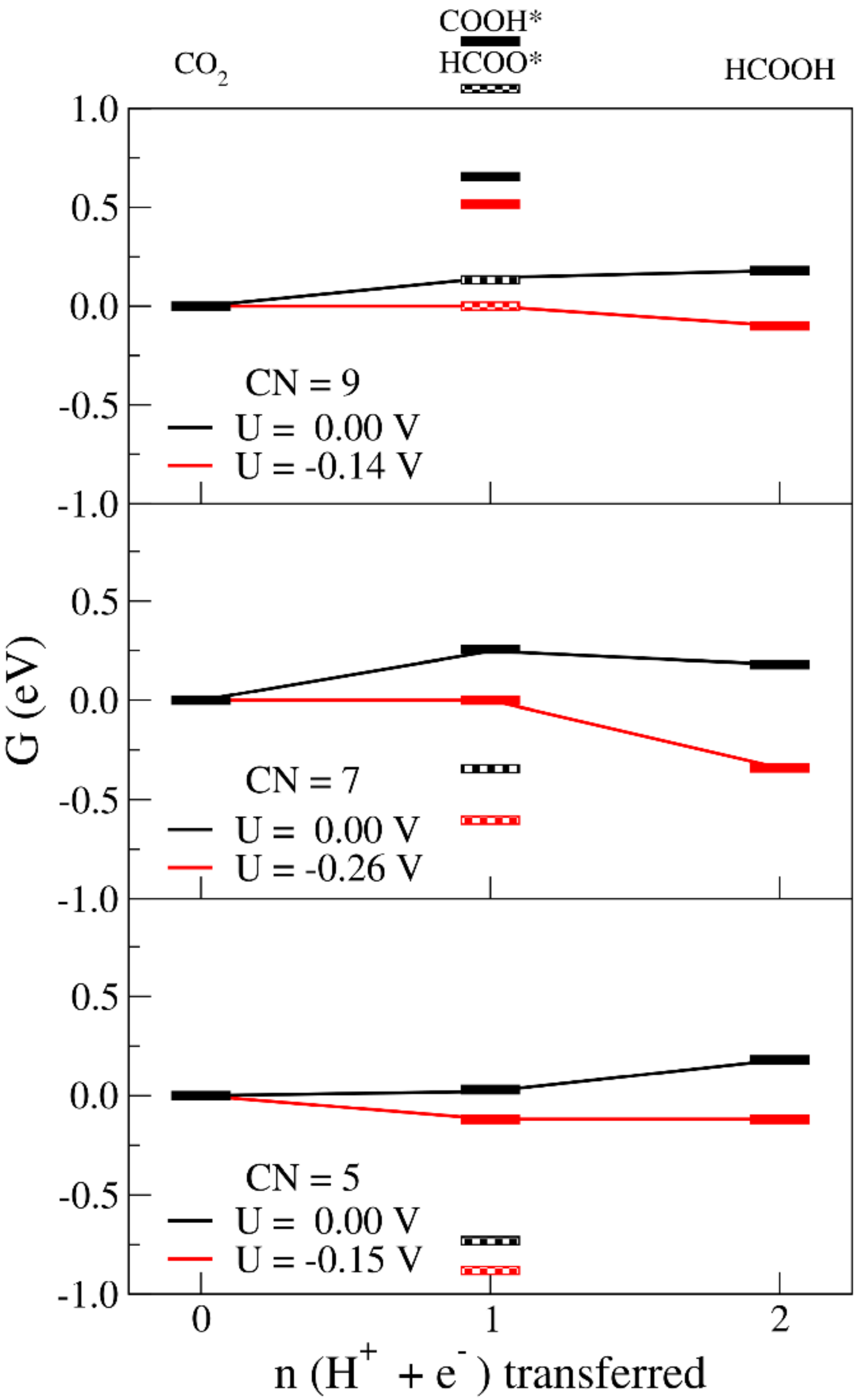

Figure S26: Free energy diagrams for CO_2 reduction towards HCOOH on regions with different levels of coordination. Black curves represent diagrams obtained for $U = 0$ (V vs RHE) while red curves represent the same diagrams calculated for the electrode potential required to allow each reaction. Solvation energies for this diagram were obtained from the work of Peterson *et al.*.[15] The reaction path with the lowest theoretical onset potential is connected with straight lines and for possible bifurcating reaction paths, the intermediates are indicated with different symbols.

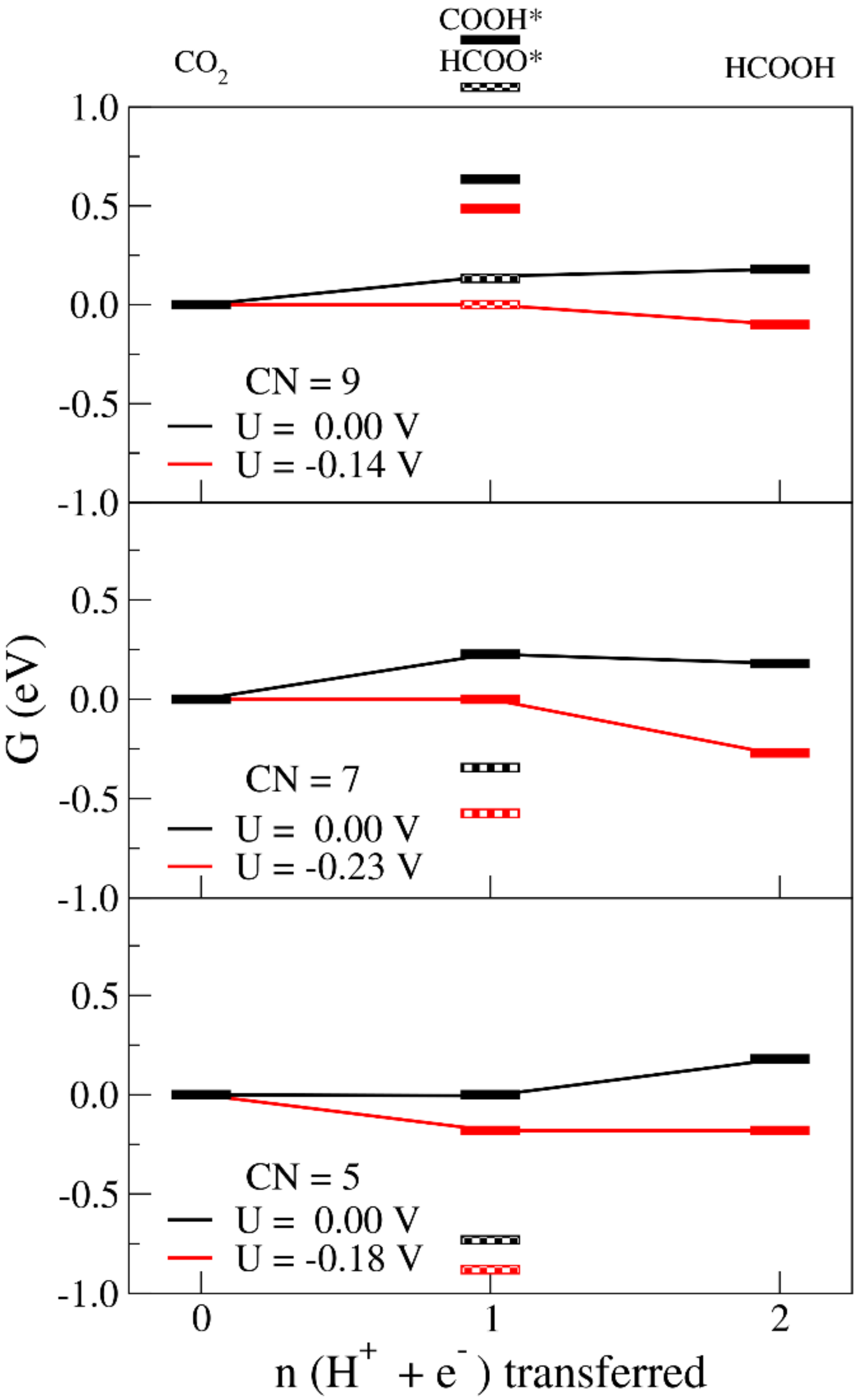

Figure S27: Free energy diagrams for CO_2 reduction towards HCOOH on regions with different levels of coordination. Black curves represent diagrams obtained for $U = 0$ (V vs RHE) while red curves represent the same diagrams calculated for the electrode potential required to allow each reaction. Solvation energies for this diagram were obtained from the work of Rendón-Calle *et al.*.[19] The reaction path with the lowest theoretical onset potential is connected with straight lines and for possible bifurcating reaction paths, the intermediates are indicated with different symbols.

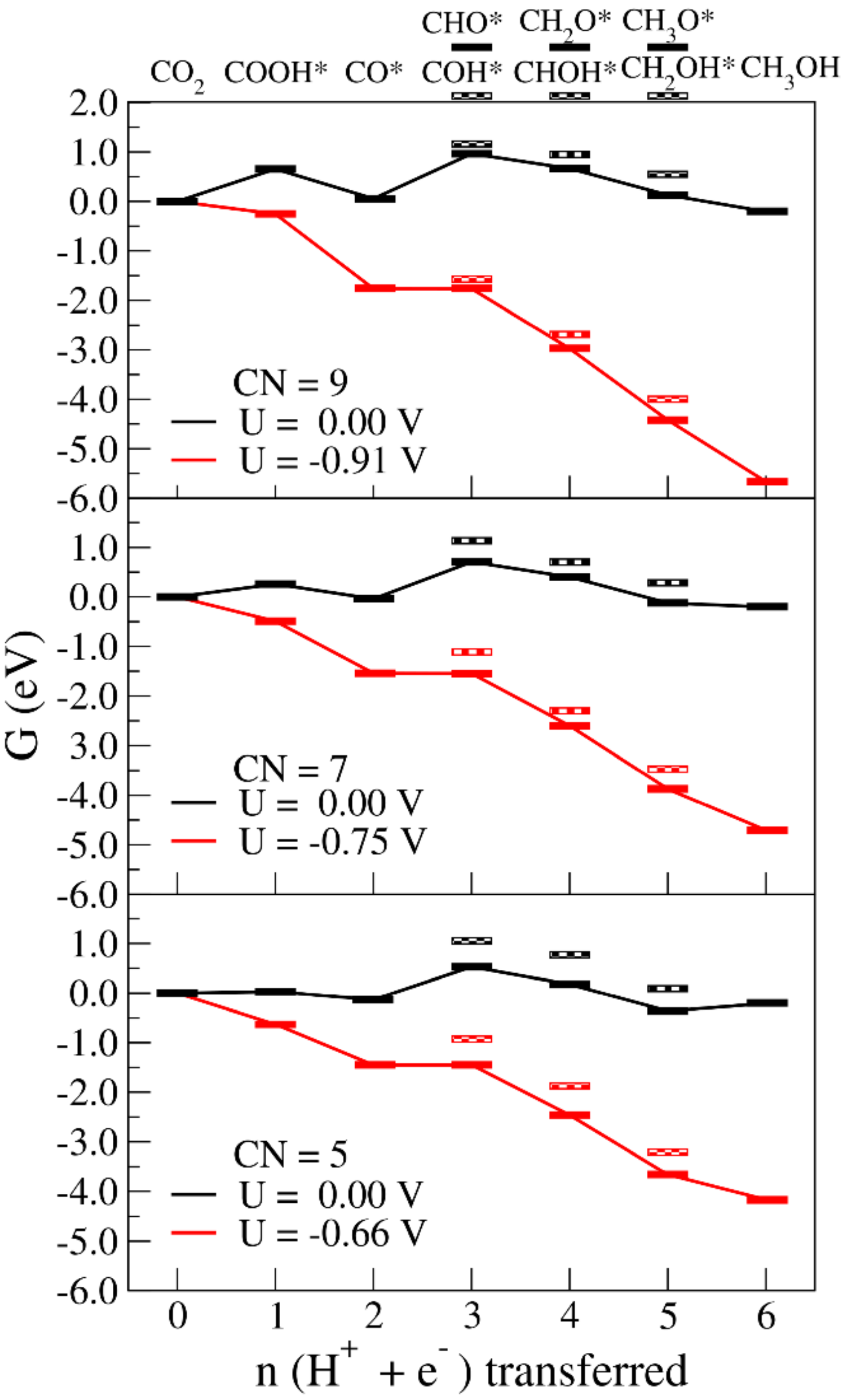

Figure S28: Free energy diagrams for CO_2 reduction towards CH_3OH on regions with different levels of coordination. Black curves represent diagrams obtained for $U = 0$ (V vs RHE) while red curves represent the same diagrams calculated for the electrode potential required to allow each reaction. Solvation energies for this diagram were obtained from the work of Peterson *et al.*.[15] The reaction path with the lowest theoretical onset potential is connected with straight lines and for possible bifurcating reaction paths, the intermediates are indicated with different symbols.

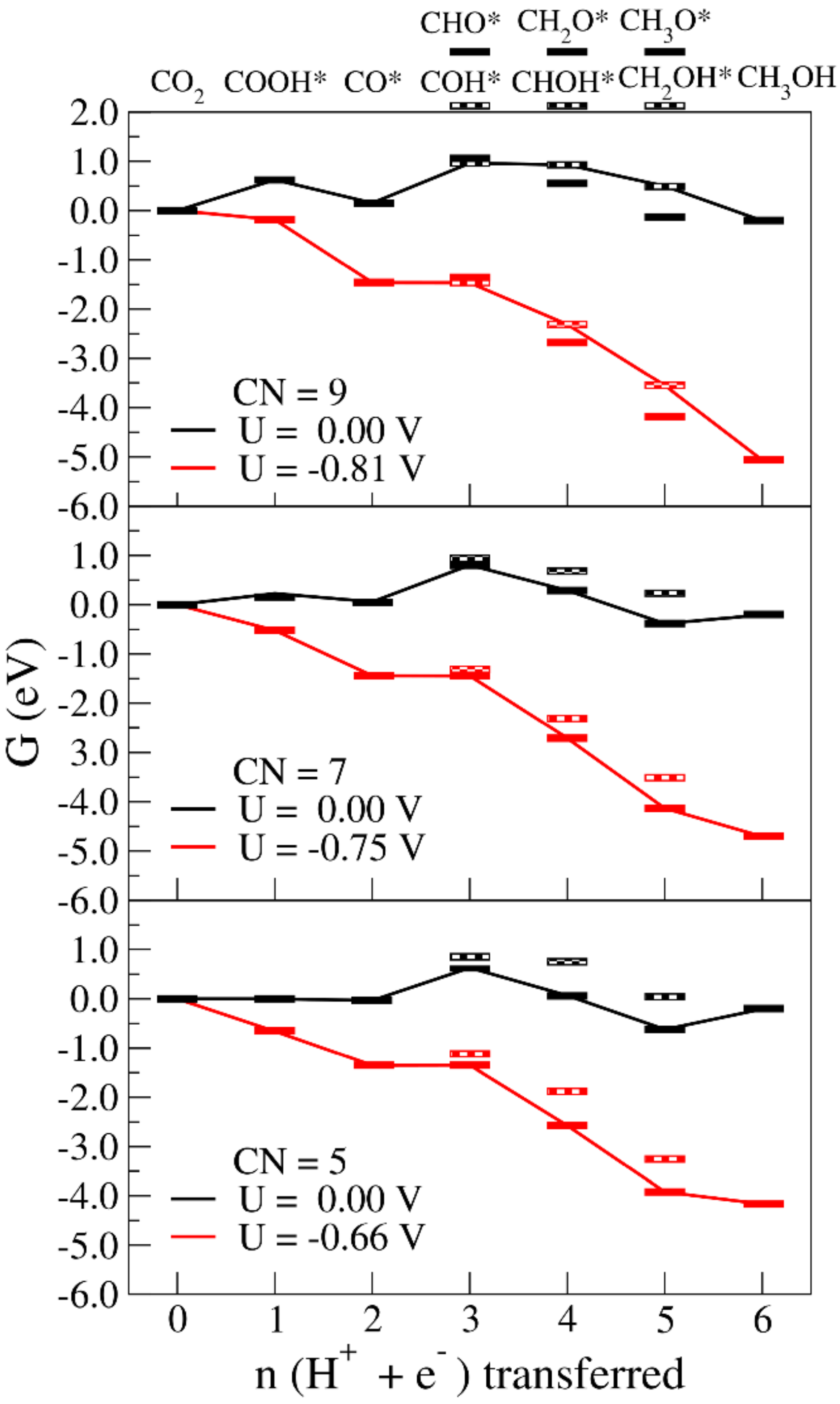

Figure S29: Free energy diagrams for CO_2 reduction towards CH_3OH on regions with different levels of coordination. Black curves represent diagrams obtained for $U = 0$ (V vs RHE) while red curves represent the same diagrams calculated for the electrode potential required to allow each reaction. Solvation energies for this diagram were obtained from the work of Rendón-Calle *et al.*.[19] The reaction path with the lowest theoretical onset potential is connected with straight lines and for possible bifurcating reaction paths, the intermediates are indicated with different symbols.

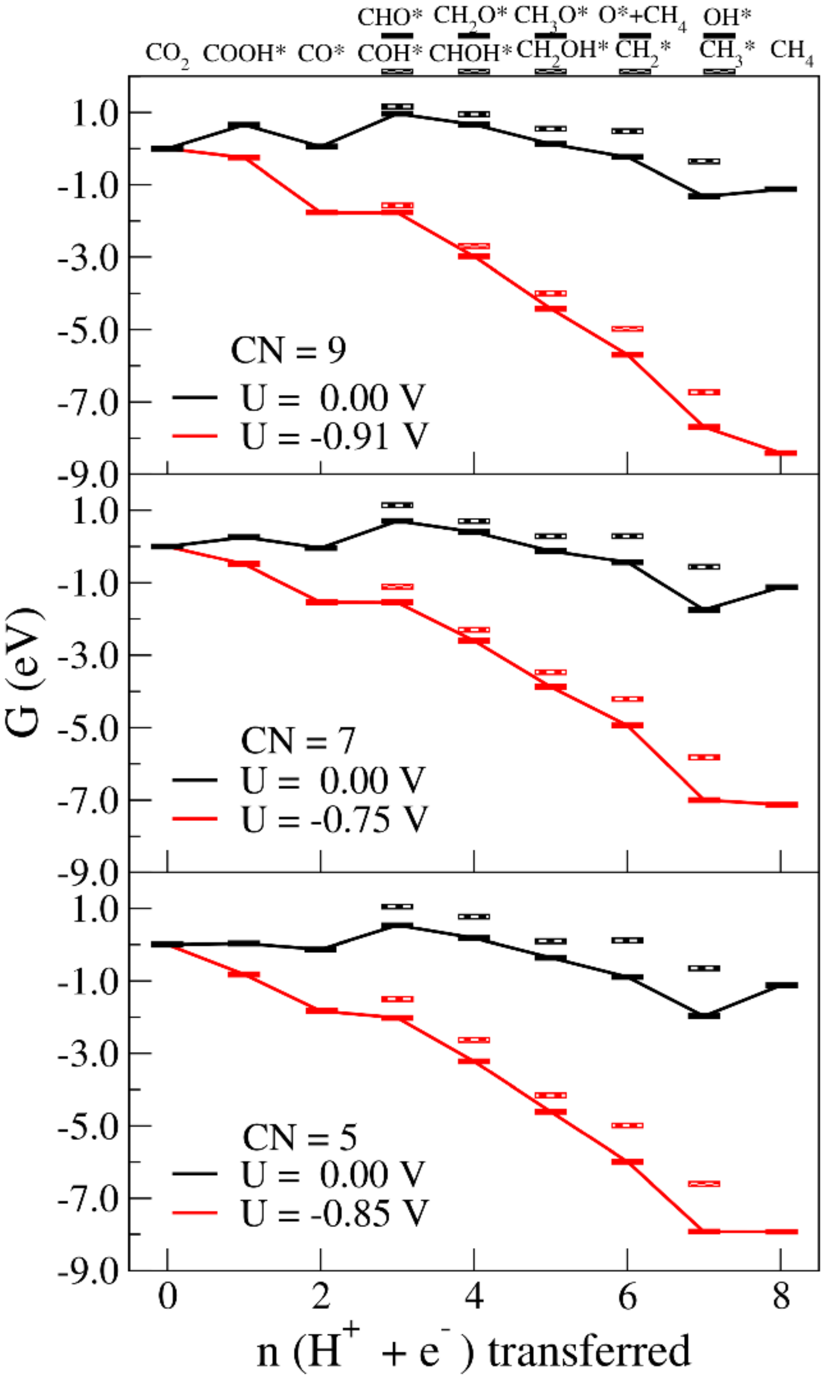

Figure S30: Free energy diagrams for CO_2 reduction towards CH_4 on regions with different levels of coordination. Black curves represent diagrams obtained for $U = 0$ (V vs RHE) while red curves represent the same diagrams calculated for the electrode potential required to allow each reaction. Solvation energies for this diagram were obtained from the work of Peterson *et al.*.[15] The reaction path with the lowest theoretical onset potential is connected with straight lines and for possible bifurcating reaction paths, the intermediates are indicated with different symbols.

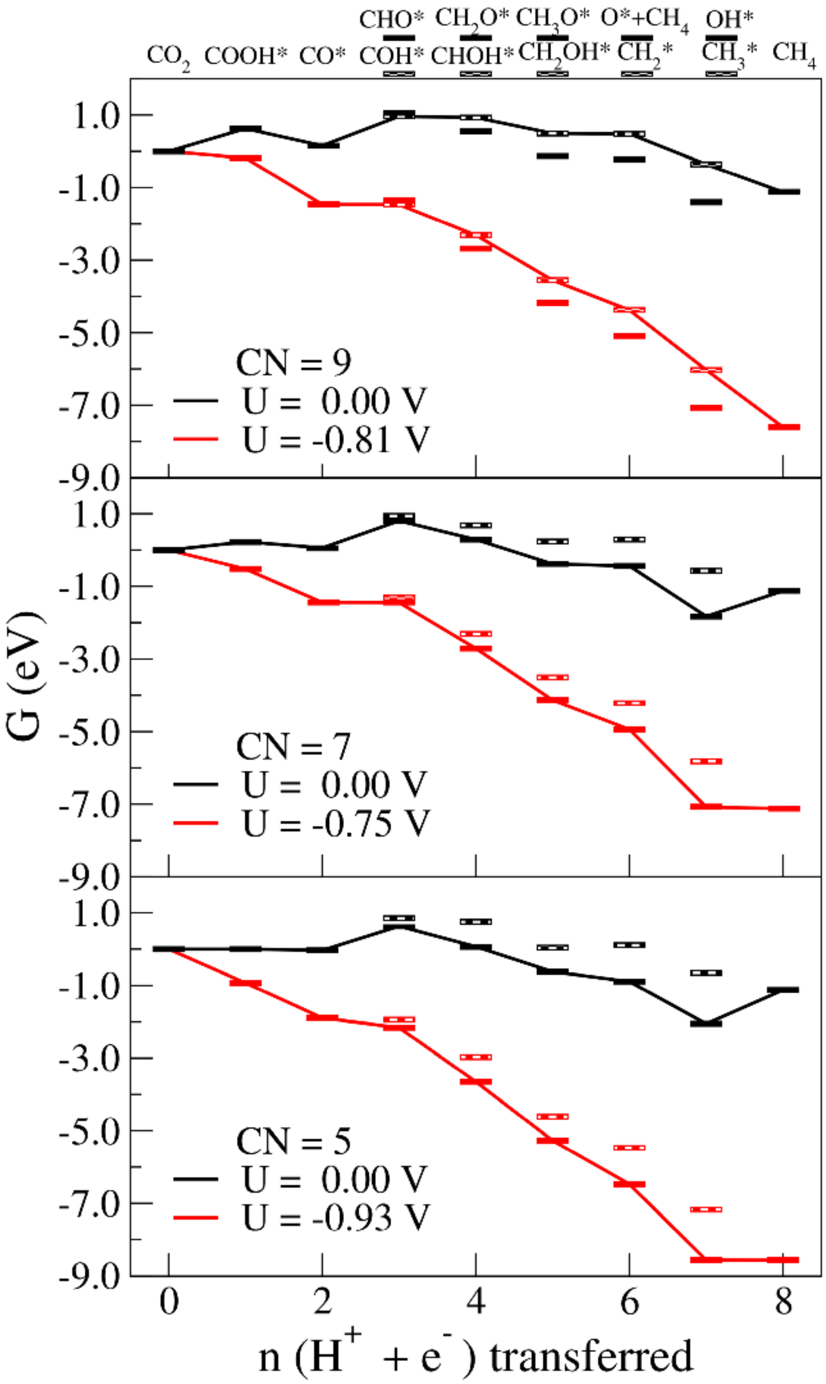

Figure S31: Free energy diagrams for CO_2 reduction towards CH_4 on regions with different levels of coordination. Black curves represent diagrams obtained for $U = 0$ (V vs RHE) while red curves represent the same diagrams calculated for the electrode potential required to allow each reaction. Solvation energies for this diagram were obtained from the work of Rendón-Calle *et al.*.[19] The reaction path with the lowest theoretical onset potential is connected with straight lines and for possible bifurcating reaction paths, the intermediates are indicated with different symbols.

References

(1) Blöchl, P. E. Projector Augmented-Wave Method. *Phys. Rev. B* **1994**, *50*, 17953–17979.

(2) Kresse, G.; Joubert, D. From Ultrasoft Pseudopotentials to the Projector Augmented-Wave Method. *Phys. Rev. B* **1999**, *59*, 1758–1775.

(3) Perdew, J. P.; Burke, K.; Ernzerhof, M. Generalized Gradient Approximation Made Simple. *Phys. Rev. Lett.* **1996**, *77*, 3865–3868.

(4) Grimme, S.; Antony, J.; Ehrlich, S.; Krieg, H. A Consistent and Accurate *Ab initio* Parametrization of Density Functional Dispersion Correction (DFT-D) for the 94 Elements H-Pu. *J. Chem. Phys.* **2010**, *132*, 154104.

(5) Da Silva, J. L. F.; Stampfl, C.; Scheffler, M. Converged Properties of Clean Metal Surfaces by All-Electron First-Principles Calculations. *Surf. Sci.* **2006**, *600*, 703–715.

(6) Da Silva, J. L. F.; Schroeder, K.; Blügel, S. First-Principles Investigation of the Multilayer Relaxation of Stepped Cu Surfaces. *Phys. Rev. B* **2004**, *69*, 245411.

(7) Lindgren, S. Å.; Walldén, L.; Rundgren, J.; Westrin, P. Low-Energy Electron Diffraction from Cu(111): Subthreshold Effect and Energy-Dependent Inner Potential; Surface Relaxation and Metric Distances Between Spectra. *Phys. Rev. B* **1984**, *29*, 576–588.

(8) Davis, H.; Noonan, J. Multilayer relaxation in metallic surfaces as demonstrated by LEED analysis. *Surf. Sci.* **1983**, *126*, 245–252.

(9) Da Silva, J. L. F.; Barreteau, C.; Schroeder, K.; Blügel, S. All-Electron First-Principles Investigations of the Energetics of Vicinal Cu Surfaces. *Phys. Rev. B* **2006**, *73*, 125402.

(10) Michaelson, H. B. The Work Function of the Elements and its Periodicity. *J. Appl. Phys.* **1977**, *48*, 4729–4733.

(11) Duan, X.; Warschkow, O.; Soon, A.; Delley, B.; Stampfl, C. Density functional study of oxygen on Cu(100) and Cu(110) surfaces. *Phys. Rev. B* **2010**, *81*, 075430.

(12) Neugebauer, J.; Scheffler, M. Adsorbate-Substrate and Adsorbate-adsorbate Interactions of Na and K Adlayers on Al(111). *Phys. Rev. B* **1992**, *46*, 16067–16080.

(13) Larsen, A. H.; Mortensen, J. J.; Blomqvist, J.; Castelli, I. E.; Christensen, R.; Dułak, M.;

Friis, J.; Groves, M. N.; Hammer, B.; Hargus, C. et al. The atomic simulation environment—a Python library for working with atoms. *Journal of Physics: Condensed Matter* **2017**, *29*, 273002.

(14) Hori, Y.; Kikuchi, K.; Suzuki, S. Production of CO and CH_4 in Electrochemical Reduction of CO_2 at Metal Electrodes in Aqueous Hydrogencarbonate Solution. *Chem. Lett.* **1985**, *14*, 1695–1698.

(15) Peterson, A. A.; Abild-Pedersen, F.; Studt, F.; Rossmeisl, J.; Nørskov, J. K. How copper catalyzes the electroreduction of carbon dioxide into hydrocarbon fuels. *Energy Environ. Sci.* **2010**, *3*, 1311–1315.

(16) Durand, W. J.; Peterson, A. A.; Studt, F.; Abild-Pedersen, F.; Nørskov, J. K. Structure effects on the energetics of the electrochemical reduction of CO_2 by copper surfaces. *Surf. Sci.* **2011**, *605*, 1354–1359.

(17) Peterson, A. A.; Nørskov, J. K. Activity Descriptors for CO_2 Electroreduction to Methane on Transition-metal Catalysts. *J. Phys. Chem. Lett.* **2012**, *3*, 251–258.

(18) Tang, M. T.; Peng, H.; Lamoureux, P. S.; Bajdich, M.; Abild-Pedersen, F. From electricity to fuels: Descriptors for C1 selectivity in electrochemical CO_2 reduction. *Appl. Catal., B* **2020**, *279*, 119384.

(19) Rendón-Calle, A.; Builes, S.; Calle-Vallejo, F. Substantial improvement of electrocatalytic predictions by systematic assessment of solvent effects on adsorption energies. *Appl. Catal., B* **2020**, *276*, 119147.